WL-TR-92-2007

ELECTRON GUN DIAGNOSTICS DEVELOPMENT

D. F. Grosjean

Systems Research Laboratories, Inc.
A Division of Arvin/Calspan
2800 Indian Ripple Road
Dayton, OH 45440-3696

April 1992

Final Report for Period 15 September 1986 - 15 October 1991

Approved for public release; distribution unlimited.

AERO PROPULSION AND POWER DIRECTORATE
WRIGHT LABORATORY
AIR FORCE SYSTEMS COMMAND
WRIGHT-PATTERSON AIR FORCE BASE, OH 45433-6563

NOTICE

When Government drawings, specifications, or other data are used for any purpose other than in connection with a definitely Government-related procurement, the United States Government incurs no responsibility or any obligation whatsoever. The fact that the government may have formulated or in any way supplied the said drawings, specifications, or other data, is not to be regarded by implication, or otherwise in any manner construed, as licensing the holder, or any other person or corporation; or as conveying any rights or permission to manufacture, use, or sell any patented invention that may in any way be related thereto.

This report is releasable to the National Technical Information Service (NTIS). At NTIS, it will be available to the general public, including foreign nations.

This technical report has been reviewed and is approved for publication.

Research Physicist
Advanced Plasma Research Group
Power Components Branch
Aerospace Power Division
Aero Propulsion and Power Directorate

Lowell D. Massie

LOWELL D. MASSIE
Chief, Power Components Branch
Aerospace Power Division

WILLIAM U. BORGER
Chief, Aerospace Power Division
Aero Propulsion & Power Directorate

If your address has changed, if you wish to be removed from our mailing list, or if the addressee is no longer employed by your organization please notify WL/POOC , WPAFB, OH 45433- 6563 to help us maintain a current mailing list.

Copies of this report should not be returned unless return is required by security considerations, contractual obligations, or notice on a specific document

REPORT DOCUMENTATION PAGE

Form Approved
OMB No. 0704-0188

1a REPORT SECURITY CLASSIFICATION UNCLASSIFIED	1b RESTRICTIVE MARKINGS
2a SECURITY CLASSIFICATION AUTHORITY	3. DISTRIBUTION/AVAILABILITY OF REPORT Approved for public release; distribution unlimited.
2b DECLASSIFICATION/DOWNGRADING SCHEDULE	
4 PERFORMING ORGANIZATION REPORT NUMBER(S) 5500 Final Report	5. MONITORING ORGANIZATION REPORT NUMBER(S) WL-TR-92-2007
6a NAME OF PERFORMING ORGANIZATION Systems Research Laboratories, Inc. A Division of Arvin/Calspan 6b. OFFICE SYMBOL (If applicable)	7a. NAME OF MONITORING ORGANIZATION Aero Propulsion and Power Directorate (WL/POOC) Wright Laboratory
6c. ADDRESS (City, State, and ZIP Code) 2800 Indian Ripple Road Dayton, OH 45440-3696	7b. ADDRESS (City, State, and ZIP Code) Wright-Patterson Air Force Base, OH 45433-6563
8a NAME OF FUNDING/SPONSORING ORGANIZATION 8b. OFFICE SYMBOL (If applicable)	9. PROCUREMENT INSTRUMENT IDENTIFICATION NUMBER F33615-86-C-2647
8c. ADDRESS (City, State, and ZIP Code)	10. SOURCE OF FUNDING NUMBERS PROGRAM ELEMENT NO. 63221C; PROJECT NO. 1D01; TASK NO. 00; WORK UNIT ACCESSION NO. 07

11. TITLE (Include Security Classification)
ELECTRON GUN DIAGNOSTICS DEVELOPMENT

12. PERSONAL AUTHOR(S)
Grosjean, D. F.

13a. TYPE OF REPORT	13b. TIME COVERED	14. DATE OF REPORT (Year, Month, Day)	15. PAGE COUNT
Final	FROM 86 Sep 15 TO 91 Oct 15	1992 April	69

16. SUPPLEMENTARY NOTATION

17. COSATI CODES			18. SUBJECT TERMS (Continue on reverse if necessary and identify by block number)
FIELD	GROUP	SUB-GROUP	Electron-Beam Diagnostics, Electron Gun, High-Voltage Diode, High-Vacuum Bushing, Ultrahigh Vacuum, Pulsed Power
20	07		
09	01		

19. ABSTRACT (Continue on reverse if necessary and identify by block number)

Two vacuum-diode facilities suitable for test and evaluation of thermionic cathodes and photocathodes were constructed. One facility has been operated at pulsed voltages of ≤ 80 kV for 3.3 μsec with a 1-in-diameter electron beam. The second facility is capable of operating with 250-nsec pulses at voltages of ≤ 500 kV; up to 6 kJ is available from the power source. Diagnostic systems for high-speed current, voltage, and current-density measurements of the gap are described. Techniques for successful attainment of ultrahigh vacuum environments are also detailed, including development of a unique high-vacuum, high-voltage feedthrough.

20 DISTRIBUTION/AVAILABILITY OF ABSTRACT ☐ UNCLASSIFIED/UNLIMITED ☒ SAME AS RPT. ☐ DTIC USERS	21 ABSTRACT SECURITY CLASSIFICATION UNCLASSIFIED
22a NAME OF RESPONSIBLE INDIVIDUAL Dr. Peter Bletzinger	22b. TELEPHONE (Include Area Code) (513) 255-2923 22c. OFFICE SYMBOL WL/POOC

DD Form 1473, JUN 86 *Previous editions are obsolete.*

PREFACE

This report covers work performed during the period 15 September 1986 through 15 October 1991 under Contract F33615-86-C-2647 by the Research Applications Division of Systems Research Laboratories, Inc., A Division of Arvin/Calspan, 2800 Indian Ripple Road, Dayton, OH 45440-3696. The work discussed herein was accomplished by D. Grosjean and W. Balster. The contract was administered under the direction of the Wright Laboratory, Aero Propulsion and Power Directorate (WL/POOC), Wright-Patterson Air Force Base, OH 45433-6563, with Dr. P. Bletzinger acting as the Government Project Monitor.

The author wishes to acknowledge the technical assistance of B. Sarka of SRL and the helpful discussions and cooperation of members of the WL Aero Propulsion and Power Directorate. The editorial assistance of M. Whitaker in the preparation of this report is greatly appreciated.

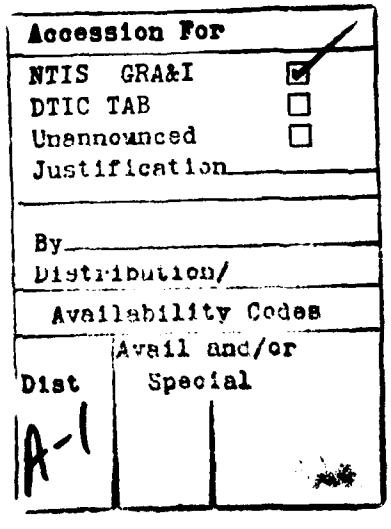

TABLE OF CONTENTS

LIST OF FIGURES

LIST OF FIGURES (Continued)

Section 1

INTRODUCTION

Electron-gun technology encompasses a variety of widely varying parameters such as electron energy, beam quality, beam brightness, and beam size. In the measurement of these parameters, painstaking procedures are often required for obtaining repeatable, reliable results--especially as voltages and currents become large and gun operation readily interferes with the performance of diagnostic systems. Often, the diagnostics must be custom made for the device since commercial equipment is either unavailable or physically unadaptable. For voltages exceeding ~ 50 kV, the attainment of accurate results can indeed be challenging.

The development of wide-area electron beams has played an important role in the advancement of laser technology.[1] Improvements in RF and photocathode-based gun systems have made significant contributions to current development efforts on free-electron lasers.[2-4] The operation of these laser systems is limited by available cathode materials. The wide-area guns typically required by laser systems must operate with uniform, large-area electron emitters; thermionic cathodes appear to be the most suitable emitter for this application. On the other hand, a promising technique for RF-accelerated free-electron lasers requires a burst of very short electron bunches of uniform energy and of good beam quality; photocathodes are showing great promise in this application.

Development of cathode materials presents even greater challenges in obtaining accurate measurements of beam parameters since the physical environment plays an important role in operating characteristics. That is, bombardment of the emitting surface by gases before, during, and after operation can seriously affect interpretation of experimental data. The diagnostics must, therefore, be compatible with a high-vacuum environment.

This report describes two test facilities constructed at Wright Laboratory for the purpose of advancing the state of the art of vacuum-diode technology, with primary emphasis on cathode-material development. One facility includes a small

ultrahigh vacuum test chamber, power sources, and diagnostics for operation of a 1-in-diameter electron-beam diode at voltages up to 60 kV. The small size of this diode allows sufficient flexibility for rapid reconfiguration; this system is, therefore, most suitable for obtaining preliminary information and identifying the most interesting parameter space of a material under test. This facility is described in Section 2.

The second facility includes a large ultrahigh vacuum chamber, power sources, and diagnostics suitable for operation of a 5-in-diameter electron-beam diode at voltages up to 500 kV. A voltage of this magnitude allows a relatively large gap spacing and high currents; however, reconfiguration is difficult and time-consuming because of the large size of the components. Section 3 contains a description of the equipment available in this facility.

Initially, emphasis in this effort was placed on construction of vacuum and diagnostic equipment for evaluation of thermionic cathodes. However, after construction was underway, interest became focused on photocathode and thermally assisted photoemitting materials. Unfortunately, budgetary constraints forced termination of the effort before significant scientific results could be obtained. Section 4 contains a brief description of the experimental setup intended for measurement of the photoelectric work function.

This report is intended as a synopsis of the work performed and the resulting capabilities of the facilities constructed. More detailed descriptions of the equipment and facilities are contained in the construction drawings and operating and service manuals which are being delivered under separate cover.

Section 2

THE 60-kV DIODE TEST FACILITY

2-1. GENERAL DESCRIPTION

Figure 2-1 is a block diagram of the major components of the 60-kV Diode Test Facility, and Fig. 2-2 is a simplified electrical schematic of the basic diode circuit. The diode is contained within a stainless-steel vacuum chamber. The diode cathode is connected to earth ground (chamber) through a current-viewing resistor, and the diode anode is connected to the positive output of a 60-kV pulse power supply.

The data-acquisition instrumentation, such as a digitizing oscilloscope and a desk-top computer system, is housed in a double-wall, RF-shielding screen room; the walls are constructed of transparent screen material, rather than solid metal sheet, to facilitate visual observation of the test area. The signal lines penetrating the screen room are either coaxial--with appropriate terminations--or fiber optic; thus, the shielding integrity of the enclosure is maintained.

The main test chamber has a total volume of ~ 45 liters; the chamber is constructed primarily of ultrahigh vacuum materials, and only cryogenic pumping is utilized. Bakeout temperature is limited to 150°C by the Kalrez[5] o-rings used for sealing various valve seats.

The 60-kV pulse power supply utilizes a lumped-element Blumlein[6] configuration switched with a pressurized spark gap. The voltage level is controlled through adjustment of the DC charging level. The pulse length is not adjustable; however, different lengths and impedances may be obtained by replacing the type-E lumped-element lines. The pulse-forming lines are designed for operation with a load impedance of 620 Ω.

Presently, the cathode configuration consists of a 1-in-diameter commercial BaO_2 dispenser cathode mounted within a uniform-field-electrode (UFE) shaped ring. This ring, in turn, is mounted onto a bellows-sealed translation

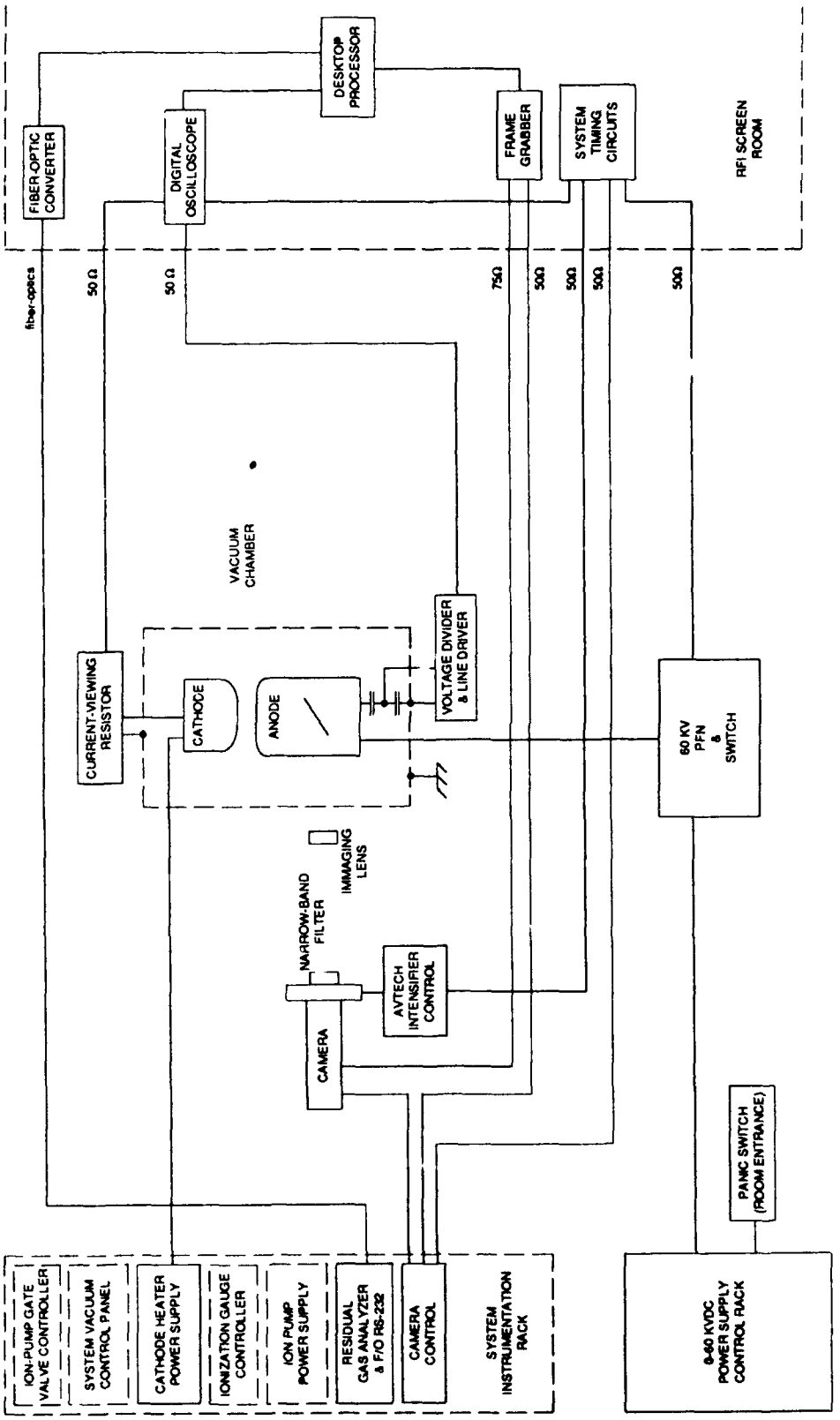

Figure 2-1. Block Diagram of 60-kV Diode Test Configuration.

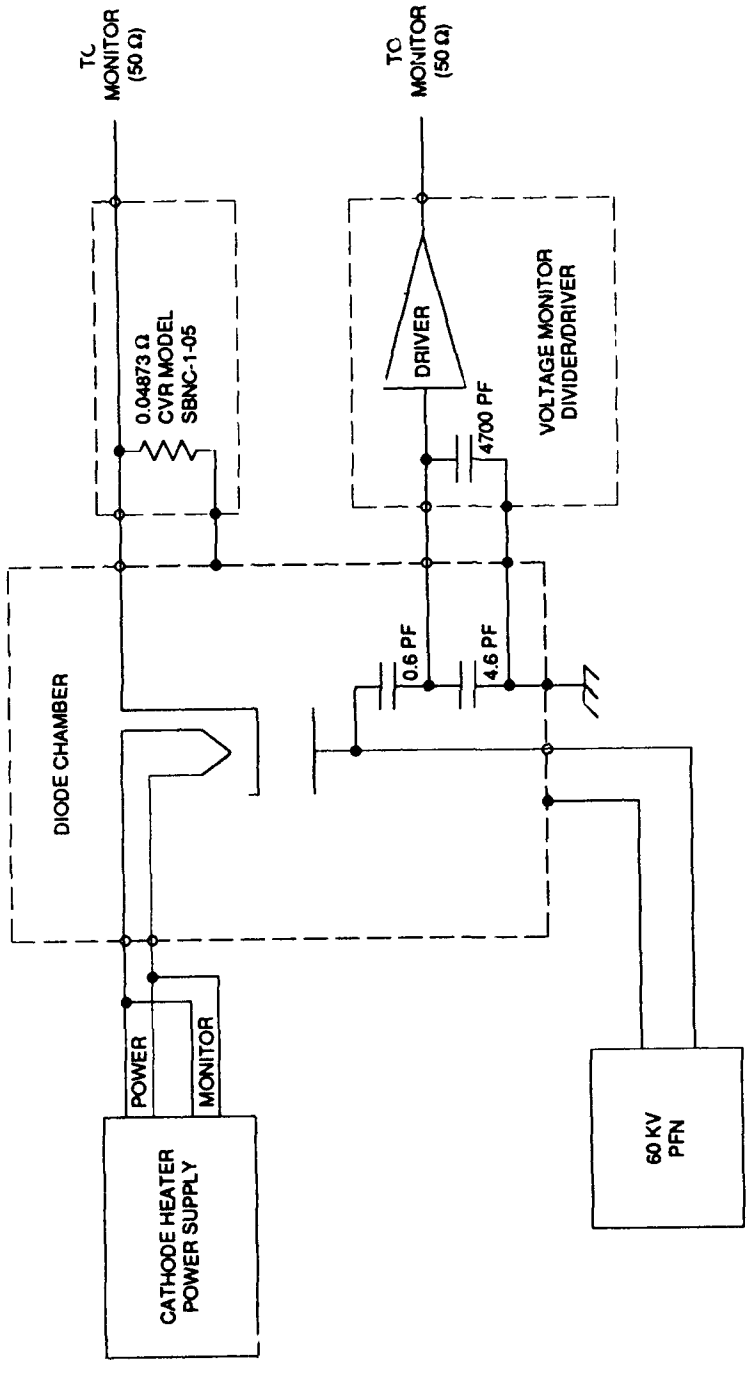

Figure 2-2. Schematic Diagram of 60-kV Vacuum Diode Circuit.

mechanism; this allows rapid and easy adjustment of the anode-cathode gap. The cathode heater is electrically isolated from the cathode and is powered by a custom-made, adjustable AC power supply. The cathode current--assumed to be the same as the gap current--is measured with a precision current-viewing resistor (CVR) and is typically monitored with a fast digitizing oscilloscope.

The system is configured with the anode as the pulsed electrode. The voltage monitor is an arrangement of high-voltage capacitors integral with the anode mounting insulators. The low-voltage leg of the capacitive divider is contained partly within the vacuum chamber and partly within an external amplifier/line-driver circuit; a high-vacuum BNC feedthrough is utilized to preserve vacuum integrity. High-input-impedance, high-speed integrated circuits are utilized to condition the signal for transmission over a 50-Ω coaxial line.

The current-density monitoring system consists of a thin molybdenum foil covering a multicrystalline BaF_2 window and a CID camera having a gated image intensifier and narrow-band optical filters. The electrons which penetrate the foil cause UV scintillation of the BaF_2. These narrow-band optical filters allow selection of the fluorescence band--one band is slow but of high conversion efficiency, suitable for setup, while the other is very fast but exhibits relatively low optical intensity. By proper adjustment of the image intensifier and synchronization electronics, a two-dimensional "picture" of the scintillation--and, therefore, the electron density--can be obtained for a selected time during a diode pulse. The picture is captured by a frame grabber and entered into the desk-top computer for subsequent processing.

2-2. A 60-kV DIODE VACUUM SYSTEM

The vacuum system was constructed primarily from commercially available hardware and equipment. A diagram of the main chamber is shown in Fig. 2-3. This custom-welded assembly is constructed from two 8-in stainless-steel four-way crosses (with 10-in flanges) connected by 6-in-diameter tubing oriented at right angles to the plane of each cross. At each end, 6-in-diameter viewports have been added on-axis with the connecting tubing. The resulting chamber has eight 8-in ports (10-in flanges) and two 6-in ports (8-in flanges). All port flanges are ultrahigh vacuum (Varian ConFlat style) compatible. One plane of

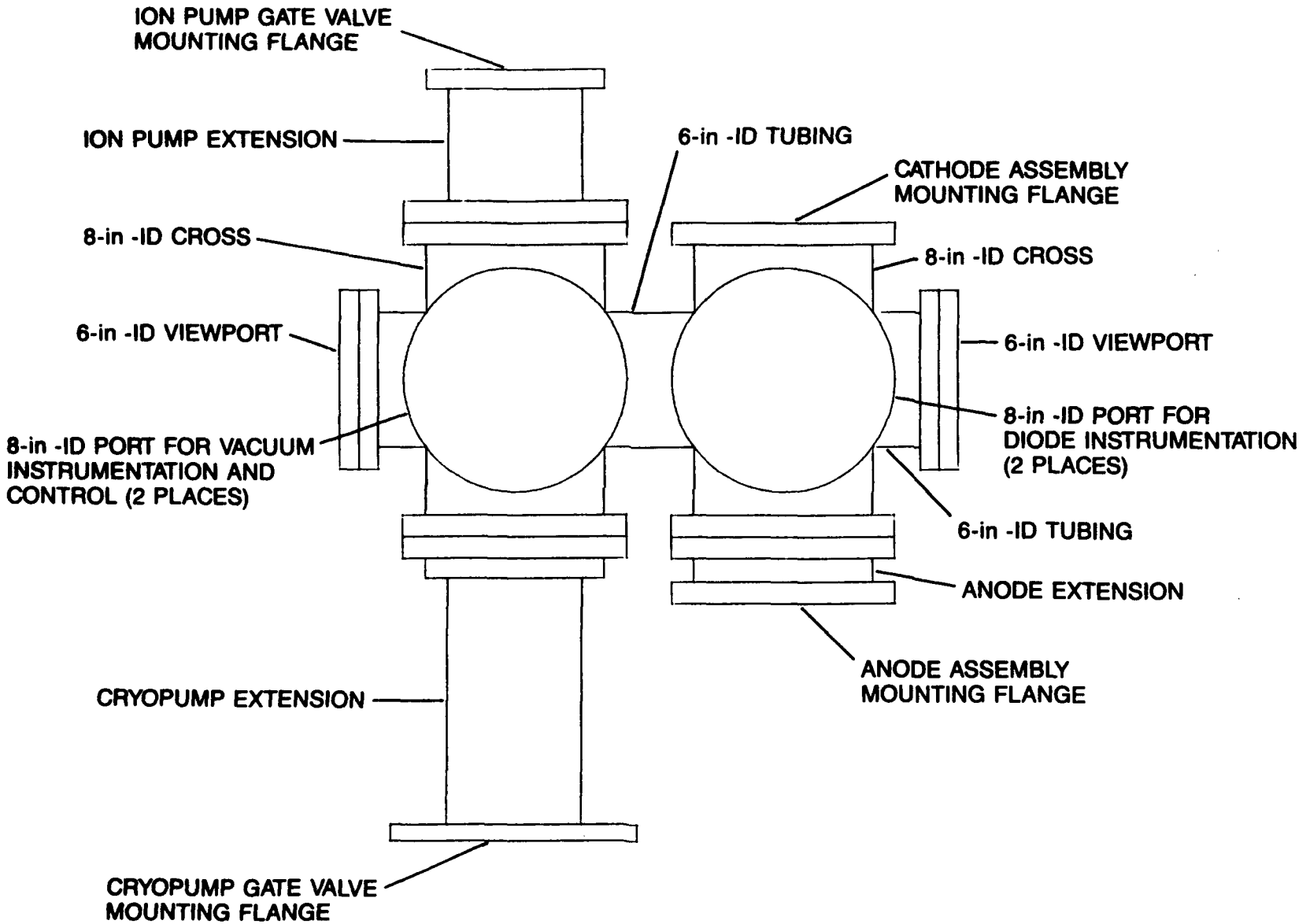

Figure 2-3. Diagram of 60-kV Diode Main Vacuum Chamber.

10-in ports is utilized for pumping equipment and vacuum instrumentation and the other contains the diode gap and associated power supply and feed-throughs for the diagnostic instrumentation.

A block diagram of the vacuum system is shown in Fig. 2-4 Rough-pumping from atmospheric pressure to < 100 mTorr is accomplished with 76,000-Torr-liter Varian VacSorb units operated with liquid nitrogen (LN_2). Two pumps are connected to the main chamber through independent, manually operated right-angle valves. These stainless-steel valves utilize metal gaskets and metal bellows for sealing to the atmosphere but contain Kalrez[5] poppet o-rings. Bakeout temperature with the valve closed is, therefore, limited to 150°C. Two pumps, rather than one, are utilized to prevent the noncondensable gases entrapped in the initial air rush from diffusing back to the chamber during pumping at lower pressures. Thus, the typical procedure for rough pumping of the chamber is to open one pump valve, listening to the initial rush of gas into the pump; when the rushing sound ceases, the valve is closed and the second pump valve is opened for pumping of the remaining gases.

The main high-vacuum pump is a Varian Cryostack 8 helium-based, two-stage cryogenic pump with a remotely located compressor. Water cooling of the compressor is accomplished with a 1-kW closed-cycle chiller (air exchange), supplemented with a low flow of laboratory water through a water-water heat-exchanger coil pair. Because of the excessive noise and vibration, the chiller and cryopump compressor are located in the basement, below the laboratory, and remotely operated via the System Vacuum Control Panel. Internal sensors and cutoffs prevent the compressor from exceeding safe operating limits of temperature and pressure.

The Cryostack 8 pump is rough pumped through its roughing port via a third Varian VacSorb pump and right-angle valve combination. Only one pump is utilized because of the relatively small volume. The vacuum control system includes a provision for semiautomatic operation of a room-temperature N_2 purge of the cryopump. Electrical interlocks prevent opening of the purge solenoid valve when the cryopump gate valve is open.

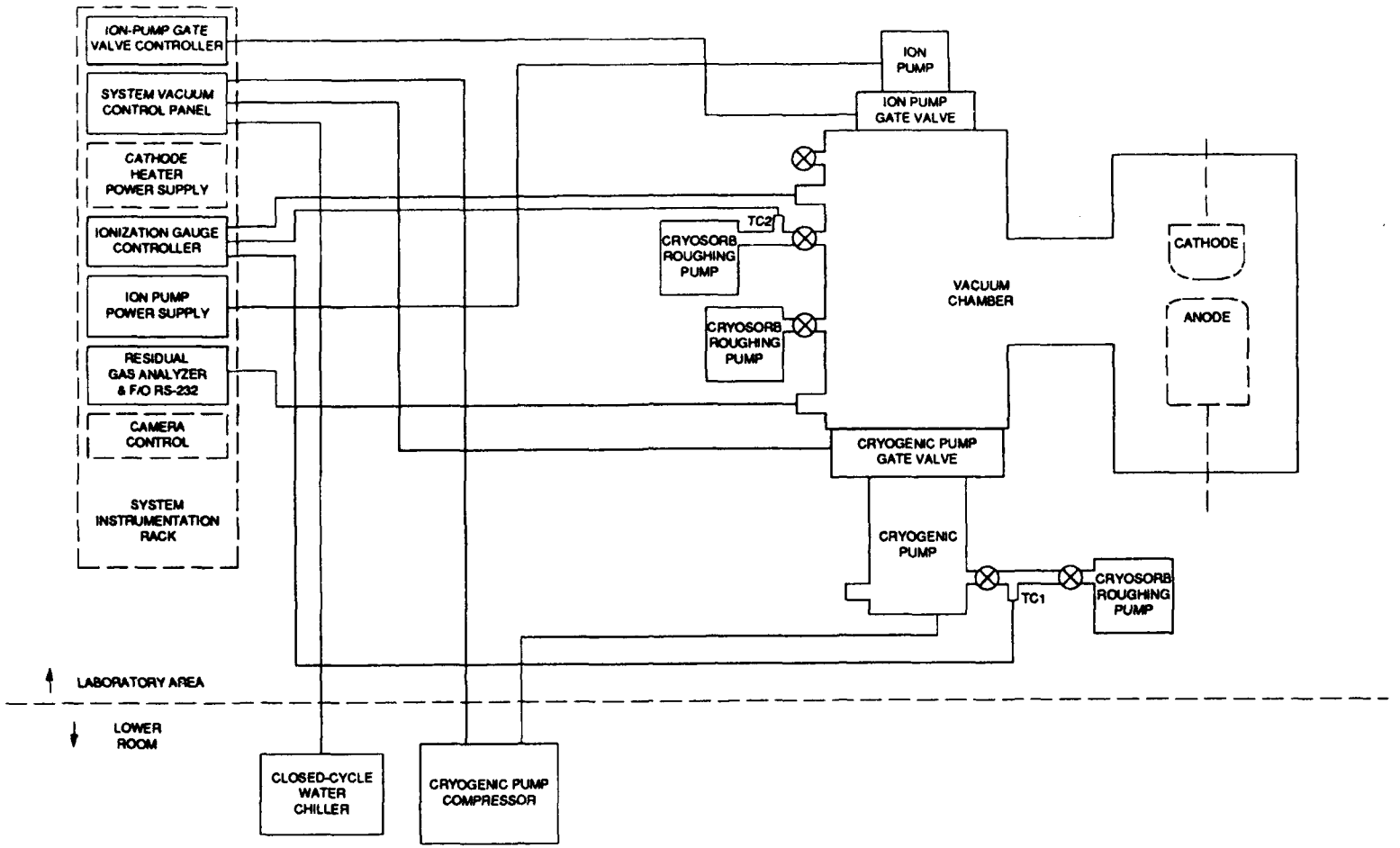

Figure 2-4. Block Diagram of 60-kV Diode Vacuum-System Monitors and Controls.

The System Vacuum Control Panel is custom made, with electrical circuitry for coordination and control of the commercial vacuum pumps and valves. The logic and control circuits are shown in the electrical schematic of Fig. 2-5. Go/no-go operation of the cryogenic vacuum pump is determined by the temperature-monitoring circuit through the factory-installed temperature-detection diode mounted on the second stage of the Varian Cryostack 8.

The theory of operation of the System Vacuum Control Panel is relatively straightforward. This panel controls the following components: 1) a Neslab water chiller via a contactor, 2) a water solenoid which controls an auxiliary water-water heat exchanger, 3) the Cryostack compressor (and, therefore, the cryogenic pump), 4) the main high-vacuum gate valve, and 5) the N_2 purge valve of the Cryostack 8.

The Cryostack diode-control circuit consists of a precision current regulator (op amp A2 of Fig. 2-5), a buffer amplifier (A1), a comparator (A3), and an open-circuit fault detector (A4). The outputs of the comparator and fault detector control a relay via a logic gate (and inverter) and a transistor driver; the relay provides compatibility between the low-voltage circuitry and the 115-VAC logic of the interlock and control circuits.

A 60-liter/sec triode ion pump is intended for use as a high-vacuum holding pump during periods of shutdown of the cryopump. The ion pump, isolated from the system by a bakeable metal-seal pneumatic valve, has sufficient capacity to maintain a chamber vacuum of better thar. 10^{-7} Torr during purging of the cryogenic pump and in the event that the cryogenic pump becomes inoperative during unattended periods, provided the cryopump gate valve is closed (closure is automatic if a cryopump fault is sensed). The ion pump is not capable of operating as the main pump during initial chamber pumpdown or in periods of high outgassing such as those which occur during operation of certain thermionic cathodes.

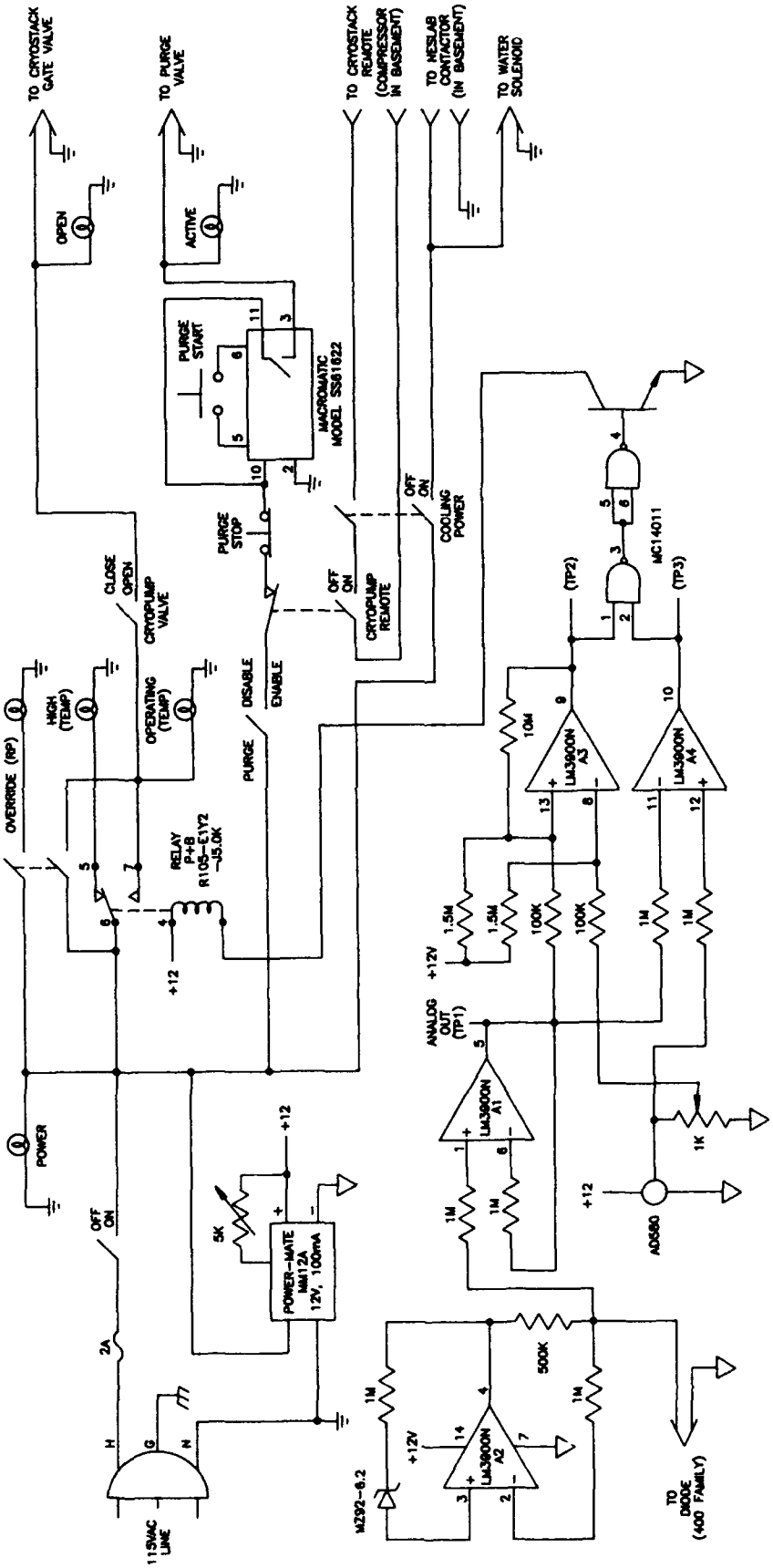

Figure 2-5. Electrical Schematic of 60-kV System Vacuum-Control Panel.

2-3. A 60-kV LUMPED-ELEMENT BLUMLEIN PULSER

The basic operating principle of the pulse power supply is shown in the block diagram of Fig. 2-6. The capacitors of the switched, type-E[6] lumped-element transmission line (left side of diagram) are charged to the level of the adjustable DC power supply through R_{CH}. The second lumped-element line (right side of diagram) is charged to the same level through R_{CH} and the path consisting of the impedance-matching resistor (R_M) and the external load. This path must be present for proper performance of the power supply.

Closure of the fast, low-impedance spark-gap switch results in a time-dependent reversal of the voltage on the connected line. This reverse voltage appears at the load end of the line a period of time after the switch is closed; this period is determined by the characteristics of the line and is presently equal to ~ 3 μsec. The time delay is especially advantageous since it allows the RFI energy resulting from the spark-gap closure to dissipate within the diagnostic circuits before the appearance of high voltage at the load.

Appearance of the reverse voltage at the load end of the switched line causes the entire second, floating, type-E line to swing to this voltage. Consequently, this reverse voltage is observed at the load. The current path for the load now consists of the two type-E lines connected in series with one leg at earth-ground potential. Because of the series connection of the lines, a "matched" load is one which has an effective impedance equal to the sum of the two lines. Essentially all of the stored energy of the lines will be transferred to the load if the effective impedance of the two lines is identical and the impedance of the total load is twice that of a single line.

If the impedance-matching conditions are not met, some energy (quantity determined by extent of mismatch) will be reflected back into the lines and appear after a time period equal to twice the line length. This reflected energy may appear as either a positive or a negative pulse--depending upon the mis-match--but is almost always an unwanted pulse. The purpose of the internal matching resistor R_M, therefore, is to set the effective resistance of the power-supply load to the proper impedance value. Presently, the matching resistor is 600 Ω, suitable for high-impedance external loads. Resistance values can be

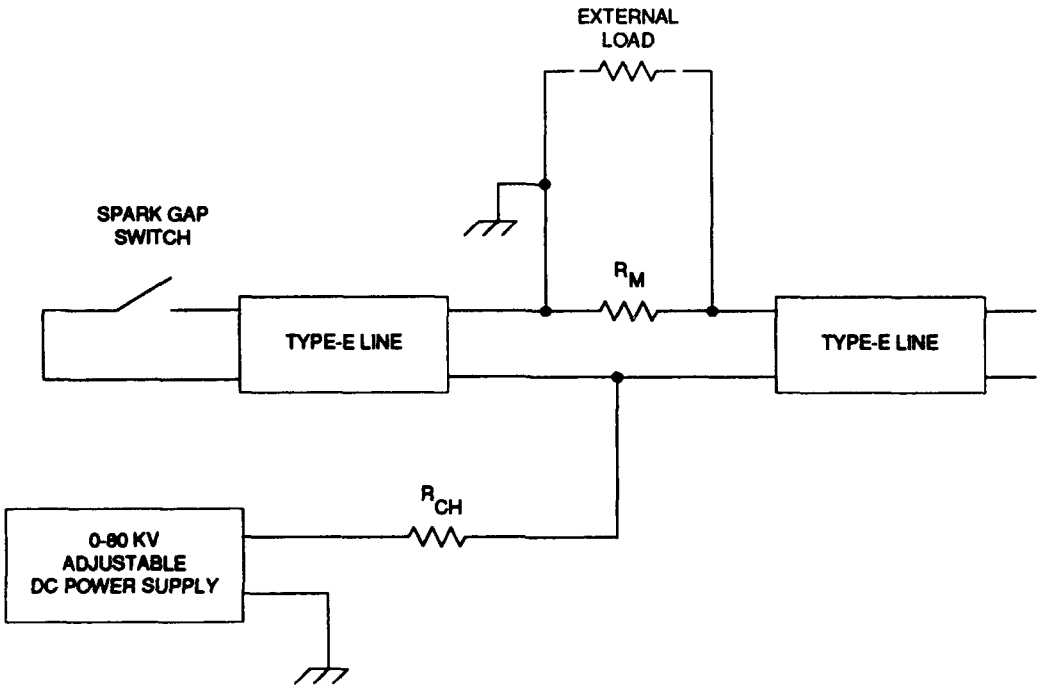

Figure 2-6. Block Diagram of 60-kV Lumped-Element Blumlein Power Supply.

changed by removing the cover of the high-voltage tank, replacing the resistor, reinstalling the cover, and purging the tank with insulating gas.

A schematic of the high-voltage lumped lines, spark-gap switch, and associated electronics is shown in Fig. 2-7. These components are installed in a metal tank which is sealed with an acrylic lid. This arrangement allows operation of the high-voltage components within an atmosphere of SF_6 insulating gas. The tank construction limits SF_6 pressures to 0.5 psig; the typical operating pressure is < 20-in H_2O. Corona-free operation was achieved for voltages up to 80 kV.

The construction of the lumped-element lines is shown in Fig. 2-8; only one line is shown since the two lines are identical. The inductors consist of a continuous length of No. 12-AWG varnished transformer wire wound on a polyvinylchloride form (machined PVC tubing). The interwinding spacing is controlled by the screw threads machined into the form, and the intercoil spacing is determined by skipping an integral number of screw threads. The commercially available capacitors utilize $SrTiO_3$ as the dielectric medium and exhibit low dissipation losses and a relatively low-voltage coefficient. The lumped-line time and impedance characteristics can be properly altered only through construction of entirely new lines; finding a practical combination of wire size, form diameter, screw spacing, and commercially available capacitor values presents a significant challenge.

The spark-gap switch was designed and constructed by government laboratory personnel and is shown in Fig. 2-9. It consists of two 1.5-in-diameter spheres separated by ~ 1 in. A 1.5-in-diameter loop, constructed of 1/8-in Cu tubing which serves as the trigger electrode is located between the spheres. This arrangement is contained within an acrylic cylindrical housing and affords a gas-tight environment. Dry laboratory air enters the housing through the tubing of the trigger ring and exits through the cylinder wall. Switching characteristics may be modified by changing the gap spacing, the relative position of the electrodes and trigger ring, and the gas content and pressure.

In order to minimize timing jitter, a commercial miniature Marx-style pulse source (Varadyne MiniMarx) was utilized as the spark-gap trigger source (see Fig. 2-7). It supplies a short, fast low-energy pulse of ~ 120 kV. A low-current

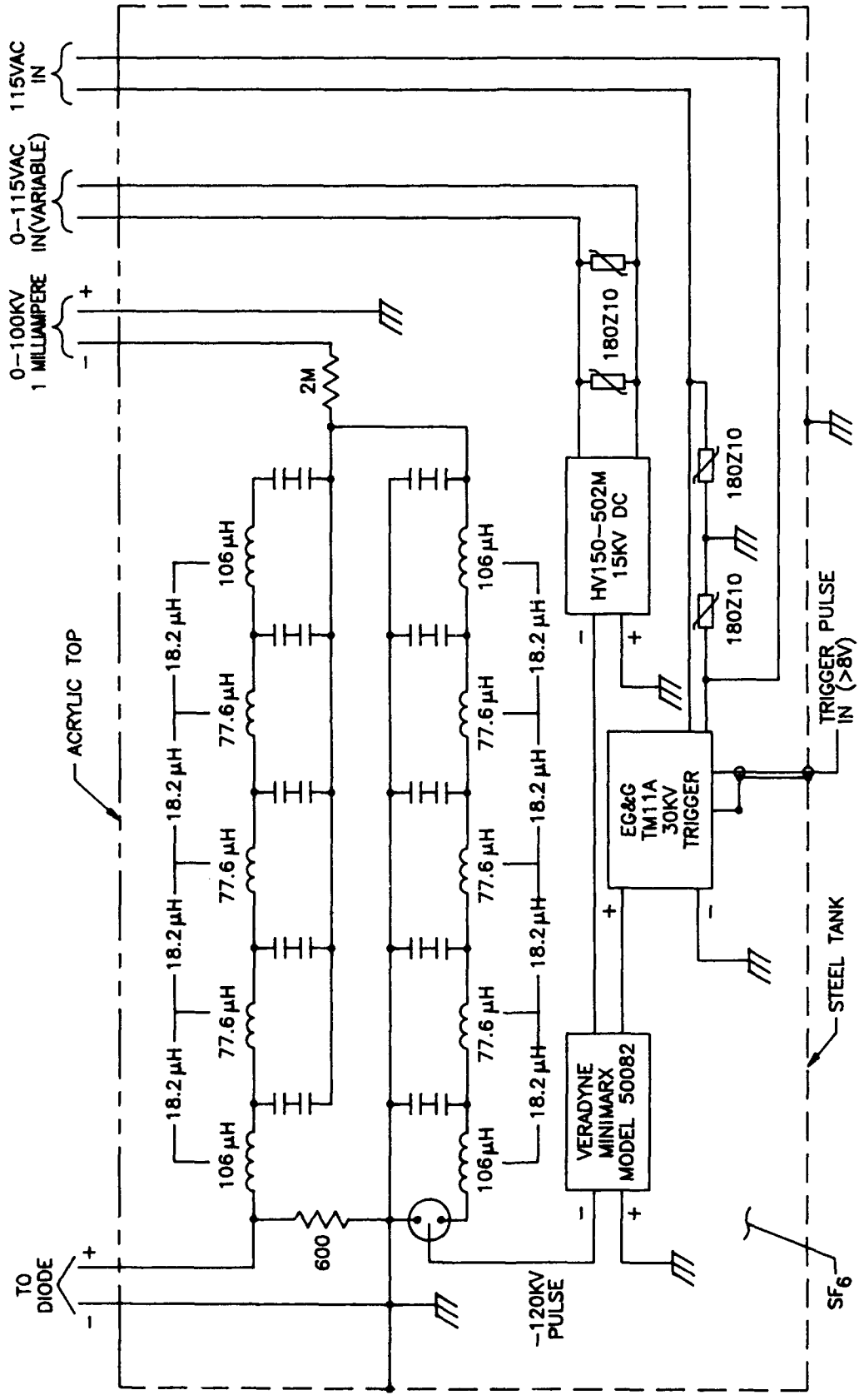

NOTES:
1. PFN INDUCTANCE VALUES ARE CALCULATED, NOT MEASURED.
2. PFN CAPACITORS ARE 2nF, 40KV.

Figure 2-7. Electrical Schematic of 60-kV Lumped-Element Blumlein Power Supply.

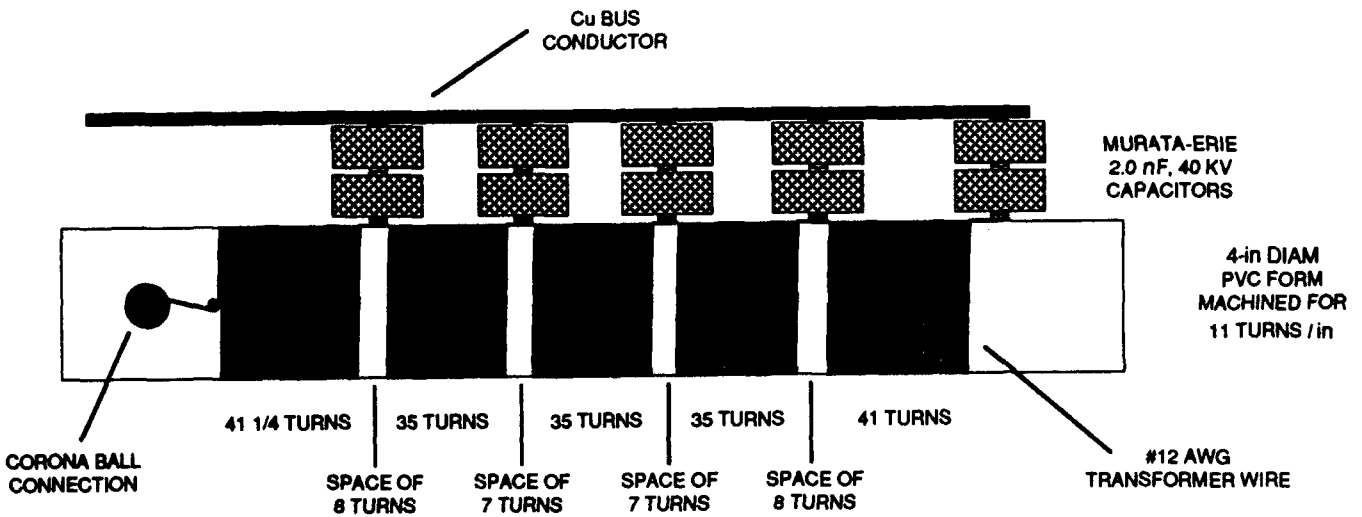

Figure 2-8. Diagram of 60-kV Lumped-Element PFN.

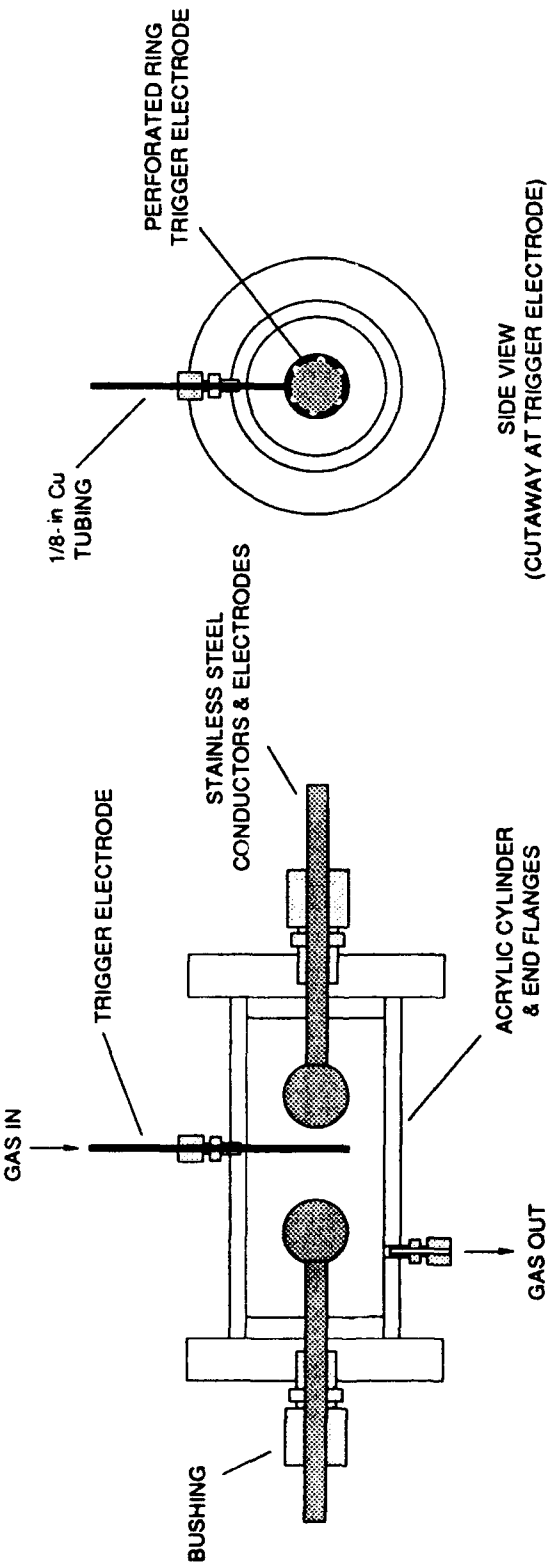

Figure 2-9. Diagram of Triggerable Spark Gap.

commercial 15-kV power source supplies the MiniMarx charging voltage; and a commercial trigger-generator, requiring a trigger pulse of ~ 15-V peak amplitude, is used to trigger the Marx unit. The MiniMarx, however, requires internal pressures > 20 psig for operation at high voltages.

Although the system is presently configured for a positive output pulse, the polarity can be changed with little effort. To accomplish this the polarity of the PFN charging supply must be reversed, and the polarity of the spark-gap trigger should be reversed. Some adjustment of the spark-gap parameters of gas pressure and trigger voltage may be necessary for optimal operation.

Figure 2-10 is a block diagram of the power sources and interlocking control circuits. The 115-VAC line power to the entire power-supply system is engaged by a latching circuit which is disabled by opening any portion of the interlock line. A safety "kill" switch, located at the main entrance of the laboratory, is included in this line; other safety-related switches can be easily added. Also, additional equipment may be interlocked with the power supply by employing the unused receptacles in the plug-strip.

2-4. CATHODE ASSEMBLY

The cathode assembly consists primarily of commercially available components. Figures 2-11 and 2-12 show two views of the assembly. The components making up the stainless-steel tubular structure between the high-current feedthrough and the cathode module are custom made, and the uniform-field-electrode (UFE) ring is custom machined. A thin tubular structure was used to minimize the heat conduction between the cathode and the vacuum feedthrough. Also, conductive heat loss by the cathode was minimized through use of three tapered screws for mounting the cathode module. A circular arrangement of stainless-steel wires carries most of the cathode current to the stainless-steel tube without significant heat being conducted.

The cathode assembly is mounted within a ring machined from pure molybdenum stock into a UFE shape. The profile was calculated from the technique of Stappaerts.[7] From the calculations a uniform electric-field distribution should exist at the electrode midplane over a diameter of 3.16 cm; the active cathode

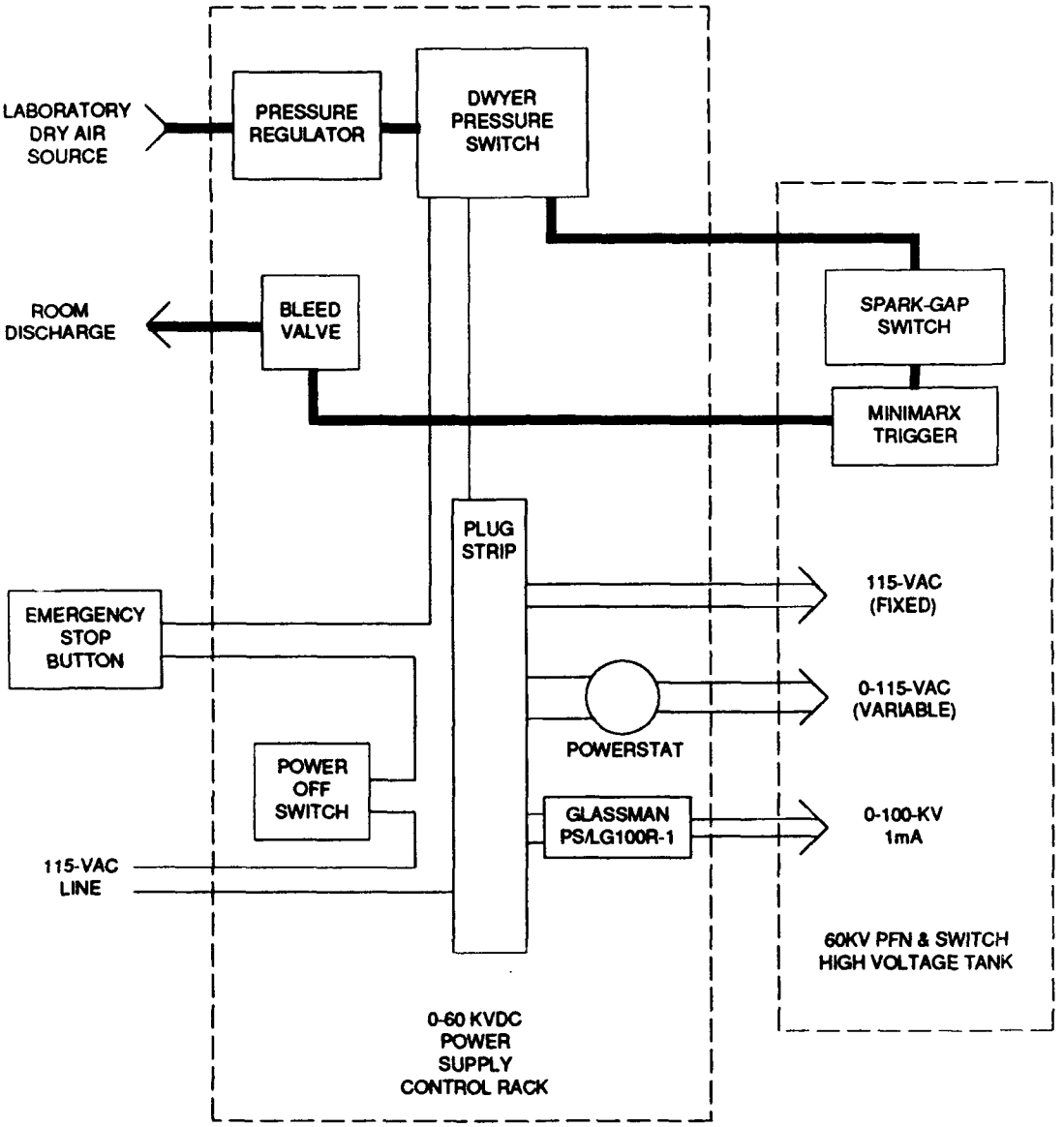

Figure 2-10. Block Diagram of 60-kV Power-Supply Control.

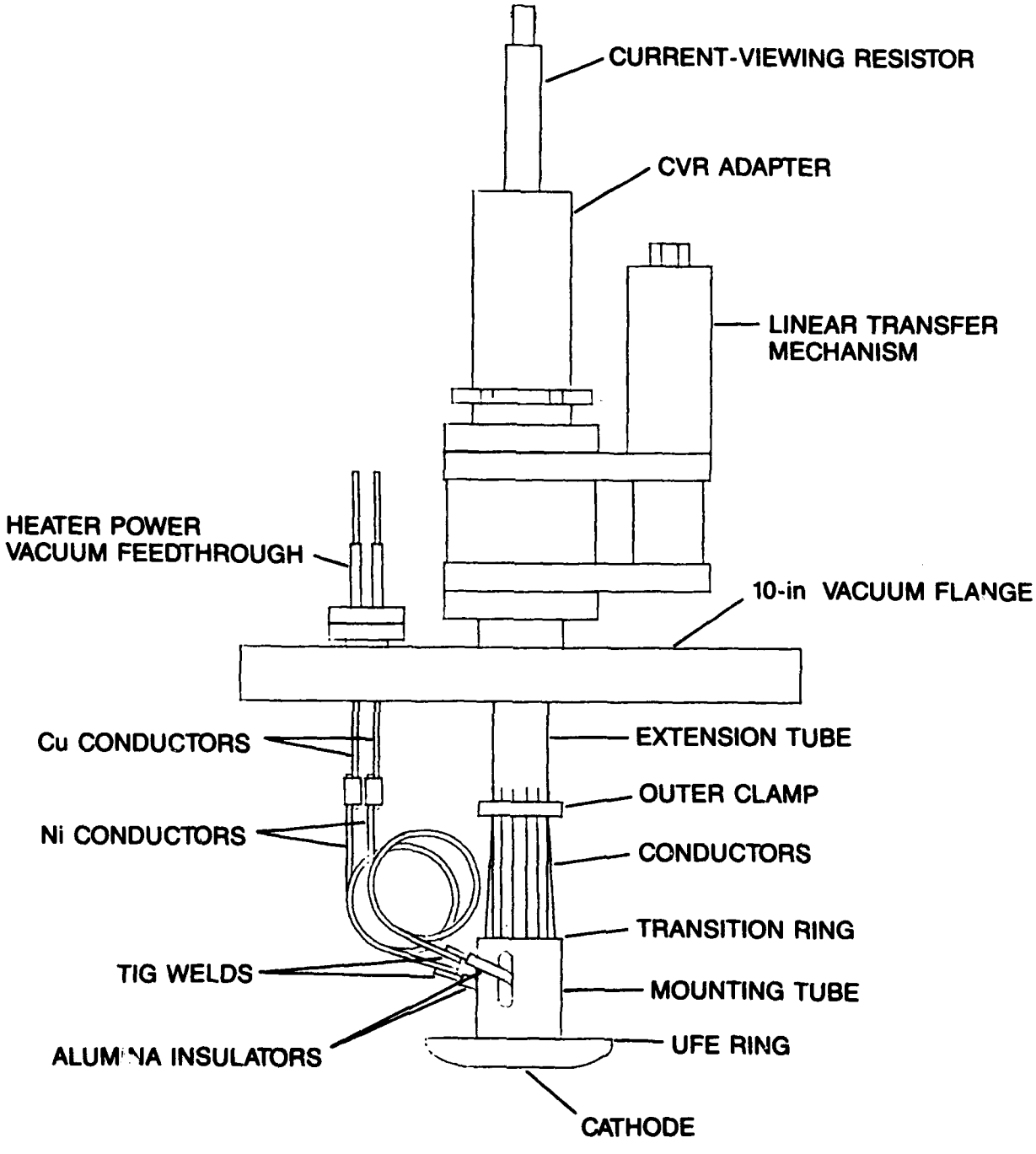

Figure 2-11. Diagram of Vacuum Diode Electrode Assembly.

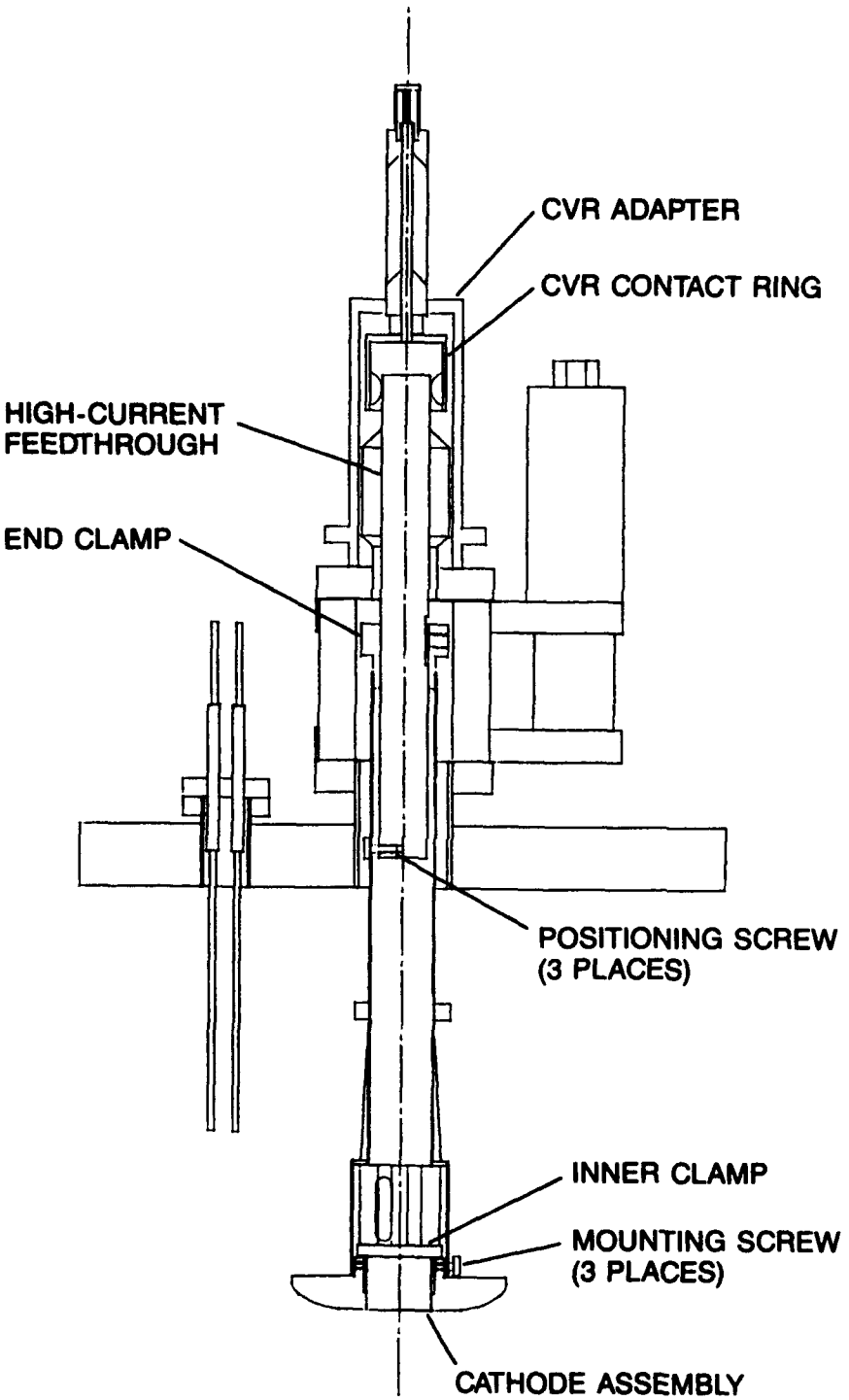

Figure 2-12. Cutaway Diagram of Vacuum Diode Cathode Assembly.

surface is 2.54 cm in diameter. For design purposes a gap dimension of 2 cm was chosen. The electrode holder was fabricated from molybdenum since the cathode manufacturer stated that Mo and Cu are the only materials which will not poison the emitting surface and Cu cannot survive the high temperatures. The holder was fabricated by a local machine shop. To preserve vacuum compatibility, only water-based aluminum-oxide polishing compounds were used and no cutting fluids were allowed.

The stainless-steel tubular structure is connected to the high-current vacuum feedthrough and isolated from the chamber by high-purity alumina. This feedthrough was chosen primarily because of its ruggedness; it is mounted to a linear translation mechanism, allowing a total travel of 5 cm. Electrically, the cathode is connected to the chamber only through the low-inductance CVR via the stainless-steel bellows and flanges of the linear transfer mechanism. The vacuum chamber provides the return current path for the diode gap.

The heater AC supply is connected to the isolated heater coil via nickel leads connected to the high-vacuum feedthrough pair; loops were added in the lines to allow for translation of the cathode. Nickel was used to facilitate the TIG-weld connection to the tungsten heater.

An electrical schematic of the AC heater supply is shown in Fig. 2-13. The circuit is relatively straightforward. Voltage and current capacity may be altered by replacing the appropriate components. No provision exists for active regulation.

2-5. ANODE ASSEMBLY

The anode assembly consists primarily of custom components. Figures 2-14 and 2-15 are diagrams of the assembly; the complete set of mechanical drawings may be consulted for details. The central 3-in-diameter portion of the anode is covered with thin (0.0002-in-thick) Mo foil which is held in place by a machined ring inserted into a 4.5-in-OD copper ring. The center 2-in-diameter portion of the disc contains a BaF_2 window. When installed into the diode vacuum chamber, this arrangement of the anode assembly allows the 1-in-diameter electron beam of the gap to strike the Mo foil, with a significant number of electrons penetrating the foil and impinging onto the BaF_2 window surface.

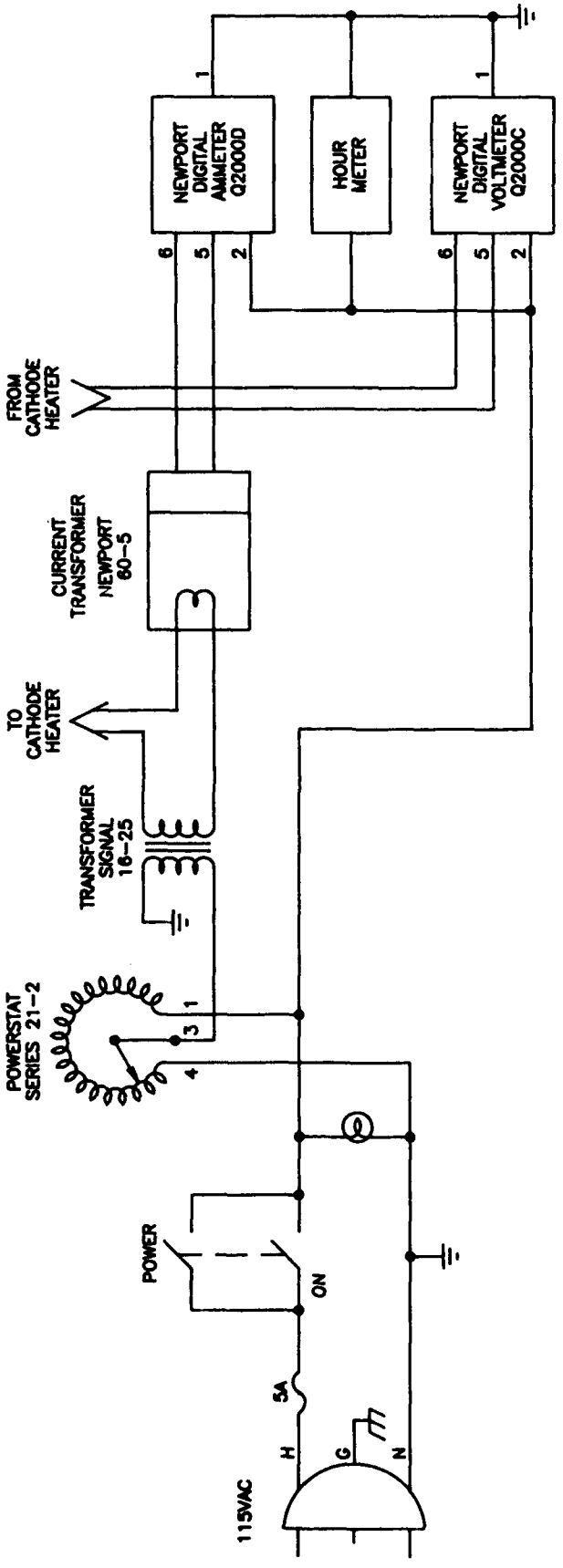

Figure 2-13. Electrical Schematic of Cathode-Heater Power Supply.

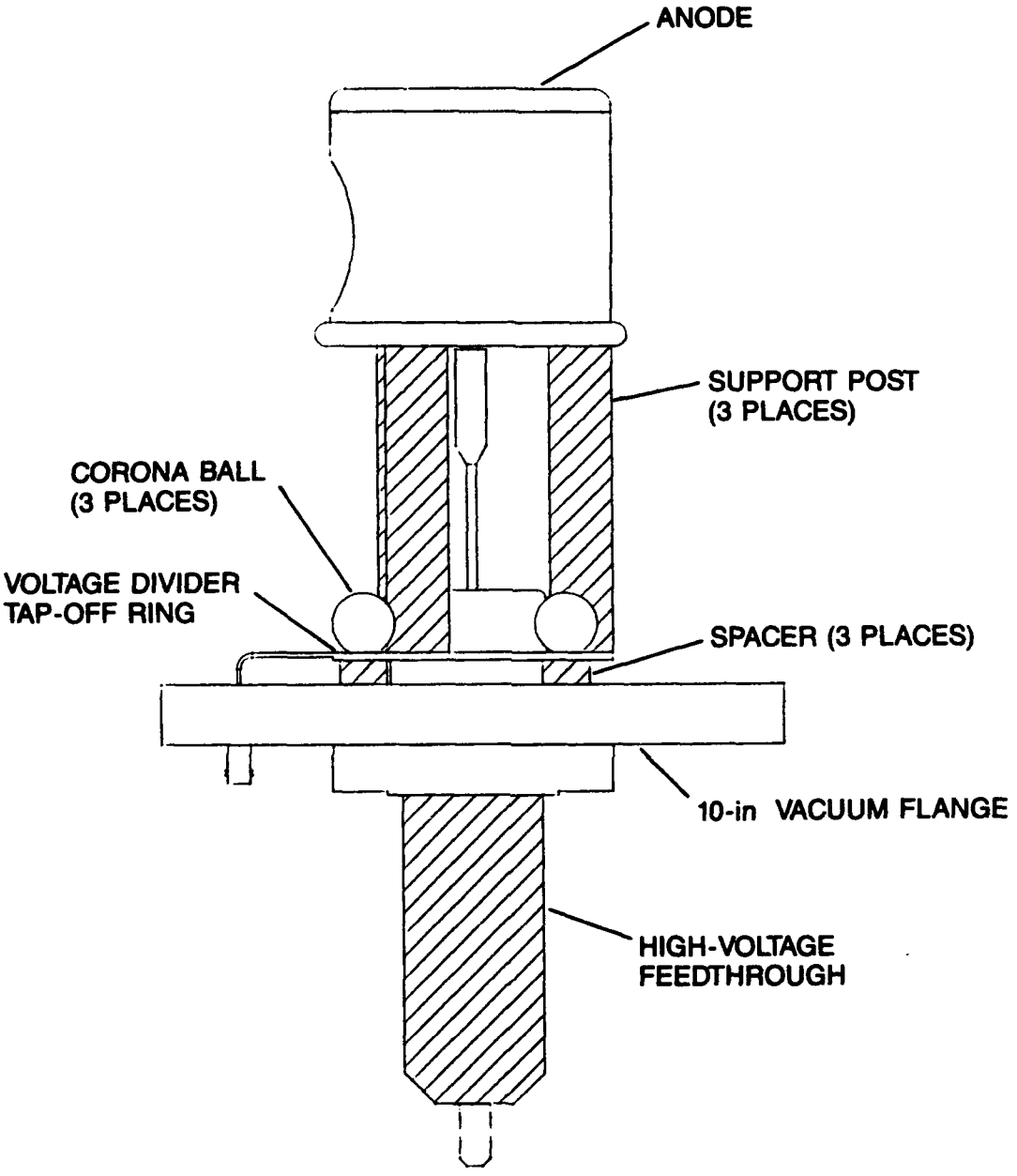

Figure 2-14. Diagram of Vacuum Diode Anode Assembly.

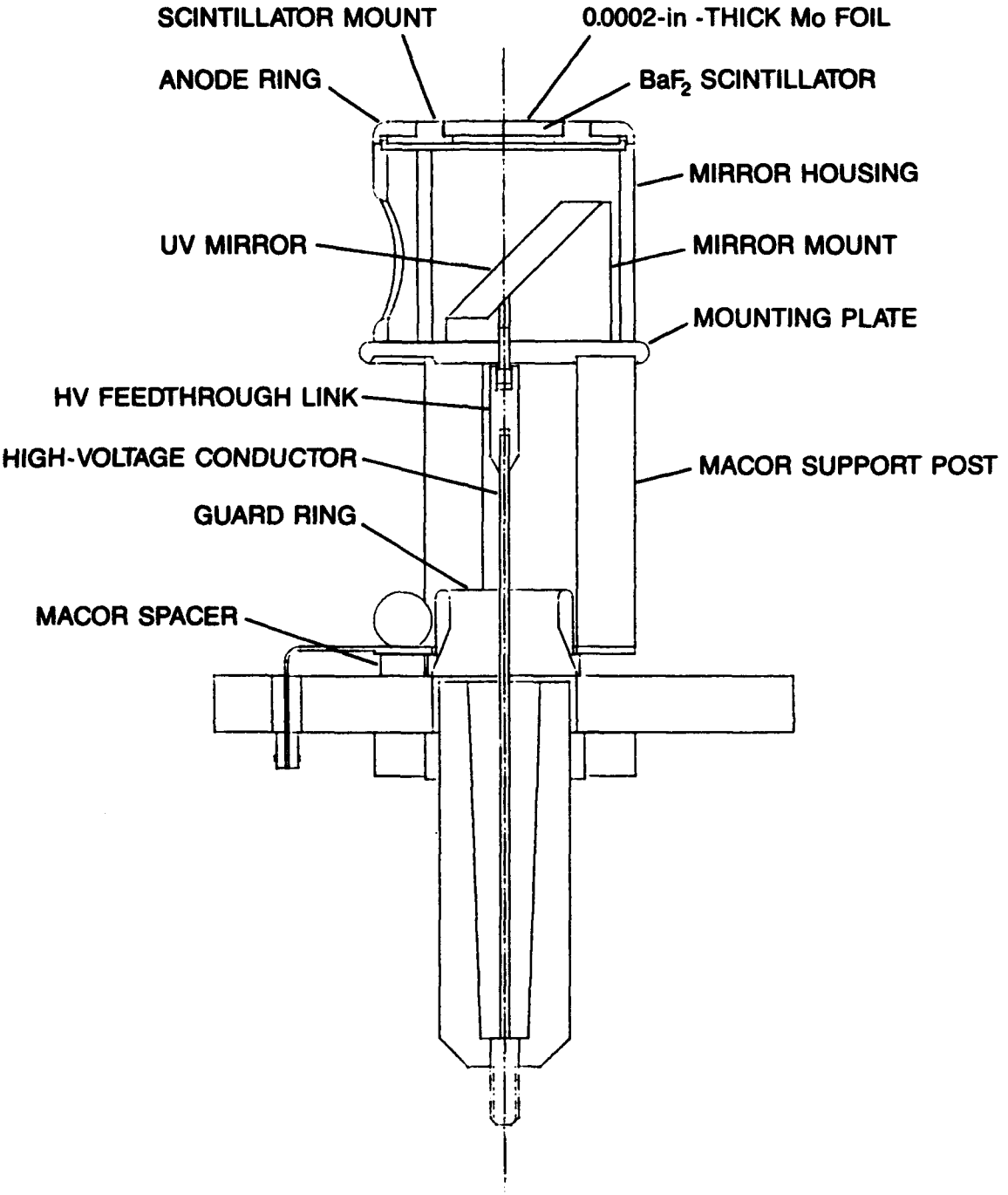

Figure 2-15. Cutaway Diagram of Vacuum Diode Anode Assembly.

The foil is positioned against the window material in order to minimize the effects of electron scattering.

A mirror, positioned at a 45-degree angle, is located below the BaF_2 window. When the mirror is properly aligned in the diode vacuum chamber, the scintillation of the BaF_2 which results from the electron beam striking the surface can be viewed outside of the chamber. Typically, a sapphire window is used as a vacuum window in order to view the fast 225-nm scintillation band. The mirror and mount are enclosed within a copper cylinder in order to prevent high-voltage corona and the arcing problems usually associated with sharp corners.

The anode cylinder is mounted on 1-in-diameter Macor[8] rods. In addition to physical support, the insulator configuration--including the voltage tap-off ring and lower spacers--forms a capacitive voltage divider with a division ratio of ~ 9:1. When assembled into the diode system, the tap-off ring is connected to an additional capacitance and a buffer/amplifier, resulting in an 8000:1 voltage monitoring system (see below).

A high-voltage, ultrahigh vacuum ceramic feedthrough is used for transmission of the anode voltage pulse. The center conductor is passed through a machined guard ring to minimize interference with the voltage divider. Although the commercially available feedthrough is rated only for 45 kV, the atmosphere side is contained within an SF_6 environment during diode operation. High-voltage breakdown has not been observed at pulsed voltages up to 80 kV.

The materials of the anode assembly are ultrahigh vacuum compatible, and custom machining was performed without oil. In addition, the surfaces in the line-of-sight of the cathode are compatible with thermionic emitters. That is, only Mo and Cu are used on the anode surface, and the Cu parts are machined from OFHC copper stock.

2-6. PULSE CURRENT AND VOLTAGE MONITORS

Total diode current is monitored with a current-viewing resistor (CVR) installed between the cathode and chamber ground. A coaxial 0.05-Ω commercial unit is used. This technique provides an accurate measure of cathode current for

the anticipated parameters of a 3.2-μsec, < 200-A pulse. Because the CVR is located in the low-voltage leg, connection to a monitor (such as an oscilloscope or a transient digitizer) is straightforward. Also, the CVR will measure only the cathode current--not stray currents which are often present at high-voltage electrodes. Here, the cathode current is of prime importance.

A voltage divider which is adequate for monitoring fast pulses of 80-kV amplitude and compatible with an ultrahigh vacuum environment is not commercially available. Since high speed is required at high voltages and since only pulse widths of < 50 μsec are of interest, a capacitive divider scheme was chosen. In order to minimize vacuum problems, the divider was designed to be an integral part of the anode-mounting arrangement.

The anode-mounting structure was discussed above (see Figs. 2-14 and 2-15 for details). The mounting rods are 5 inches in length and 1 inch in diameter, constructed of Macor, and supported by a conductive ring which, in turn, is supported by 3/8-in-long, 3/4-in-diameter Macor spacers. This forms a capacitive divider, with the capacitance of the long-rod leg being ~ 0.6 pF. The conductive ring is connected to the center conductor of an ultrahigh vacuum, BNC-style coaxial feedthrough.

External to the vacuum environment, the BNC conductor is connected to a high-speed disc capacitor which, in combination with the capacitance of the conductive ring and other stray capacitances, makes up the low-voltage leg of the voltage divider. The final division ratio is ~ 8000:1. The disc capacitor and operational amplifiers and associated electronics are contained within a shielding-metal box mounted at the BNC connector. The short connection length aids in minimizing both RFI and ground-loop problems.

A circuit schematic is shown in Fig. 2-16. The circuit output is capable of driving a 50-Ω coaxial-cable system. Extreme measures were taken during construction to achieve a very fast but stable amplifier/driver circuit. The arrangement and final value of the disc capacitor were determined empirically.

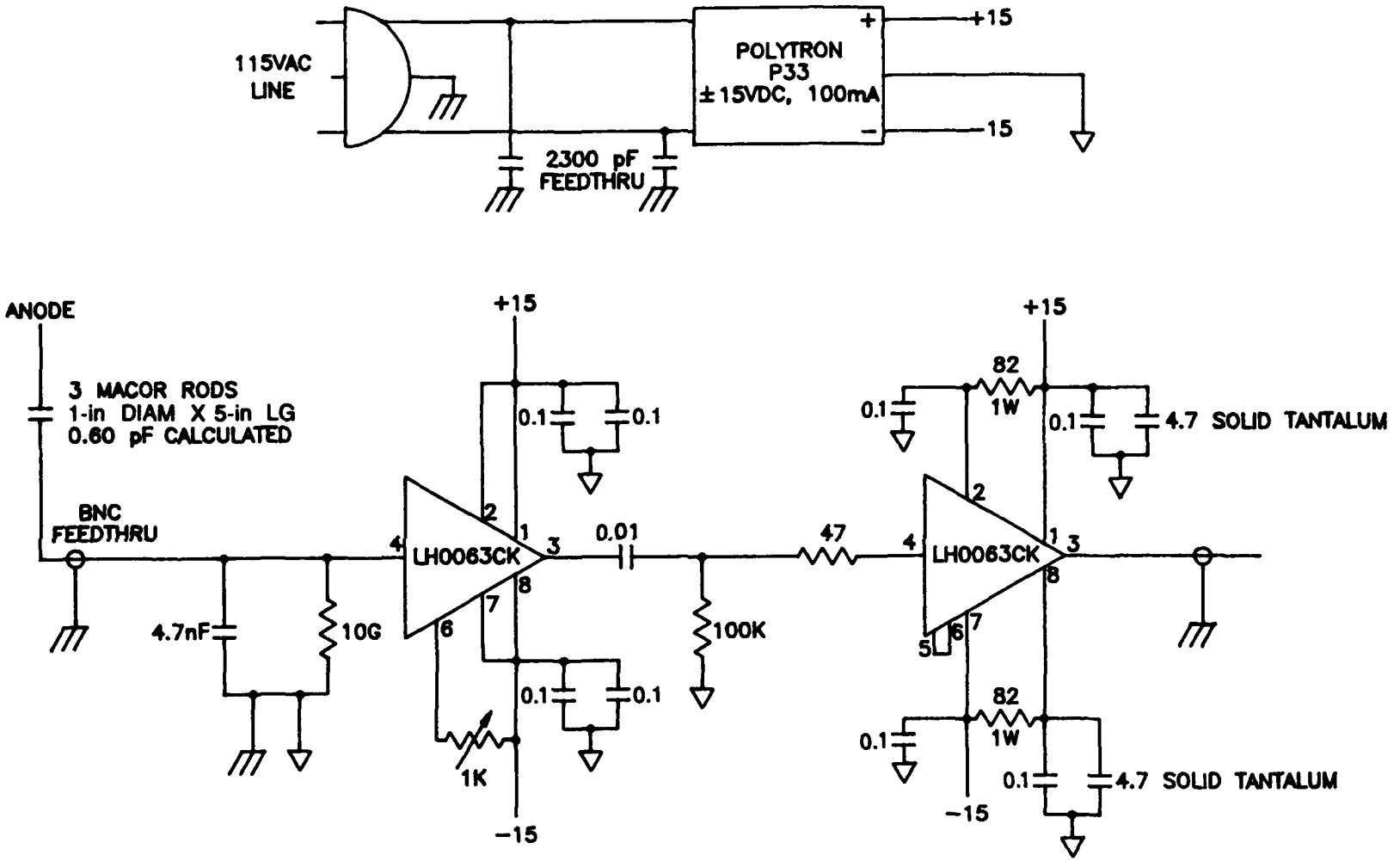

NOTES:

1. ALL CAPACITORS TO BE CERAMIC DISCS UNLESS OTHERWISE SPECIFIED.
2. ALL RESISTORS ARE 1/4W UNLESS OTHERWISE SPECIFIED.

Figure 2-16. Electrical Schematic of 60-kV Anode Voltage Divider/Amplifier Circuit.

2-7. CURRENT-DENSITY MONITOR

The block diagram of Fig. 2-1 shows the layout of the image-capture system within the total diode configuration. The external lens is employed to image the optical output of the 2-in-diameter scintillator onto the ~ 0.3-in-square active area of the intensifier. A narrow-band filter is used to select the wavelength band of interest--228-nm bandpass for fast measurements and 313-nm bandpass for higher scintillation efficiency but lower time resolution.[9]

Figure 2-17 is a more-detailed block diagram of the camera system and associated electronics. The Camera Control module supplies power to the CID camera. The rising edge of an ARM signal, or depression of the MAN TRIG pushbutton on the Camera Control front panel, initiates a sequence of events which prepares the camera for an optical signal. No light, however, can reach the camera CID sensor while the intensifier is off. A SHUTTER OPEN signal at the input of the Intensifier Control box activates the intensifier, which effectively opens the shutter. The intensifier will remain on for the time set on the Intensifier Control front panel, regardless of the duration of the SHUTTER OPEN signal. The Camera Control also signals the Frame Grabber, via the REMOTE input of the Colorado Video Model 491, to store the next video frame. This frame will contain the video information collected while the intensifier was on.

The details of the Camera Control electronics are contained in the schematic of Fig. 2-18. The circuit was designed as a "slave" to the main diode. That is, although the camera circuits contain independent timing sequences, an "arm" signal from the diode circuits causes an interruption of normal camera-scanning sequences and a rapid resetting of specific circuits. A time-window is issued by the camera circuits when conditions are proper for acceptance of a video frame. The diode synchronizing circuits are then free to trigger a diode pulse anytime within this window. Details of intensified camera operation can be found in the operating and service manuals.

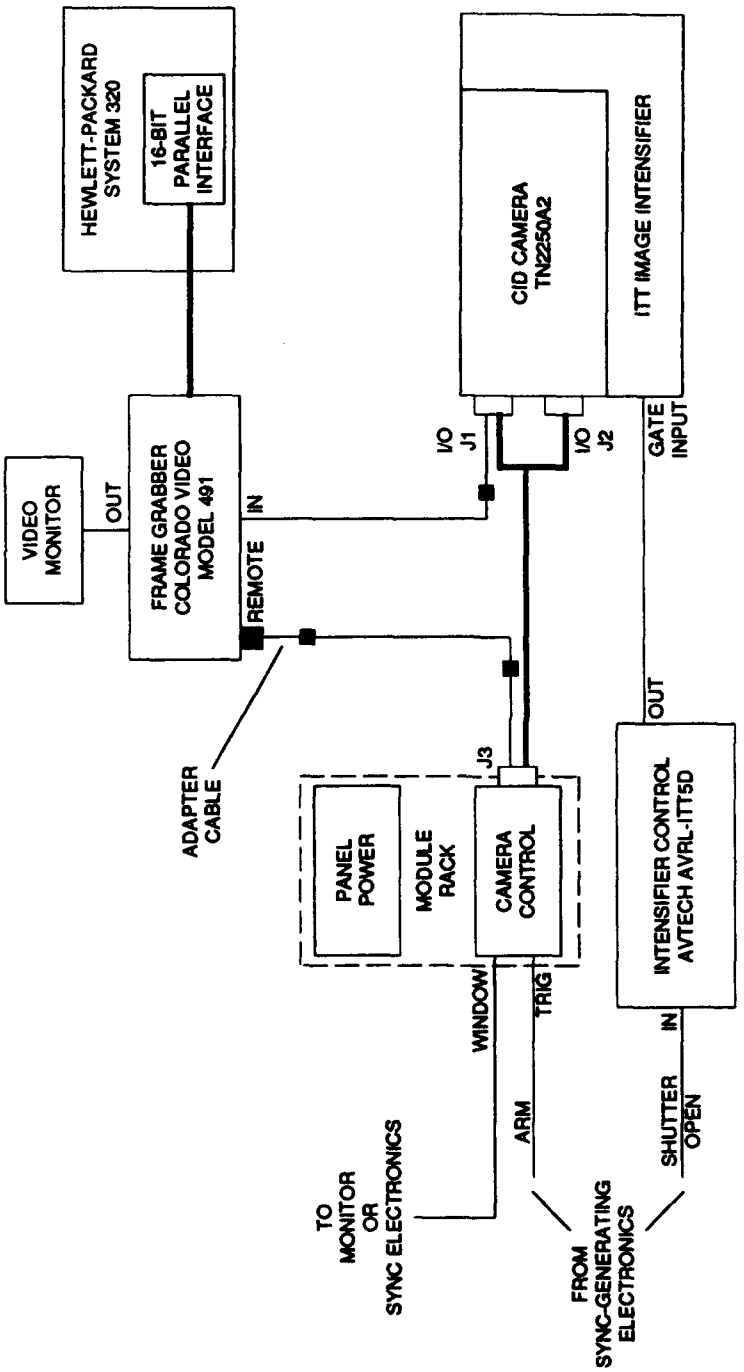

Figure 2-17. Block Diagram of Image-Capture System Configuration.

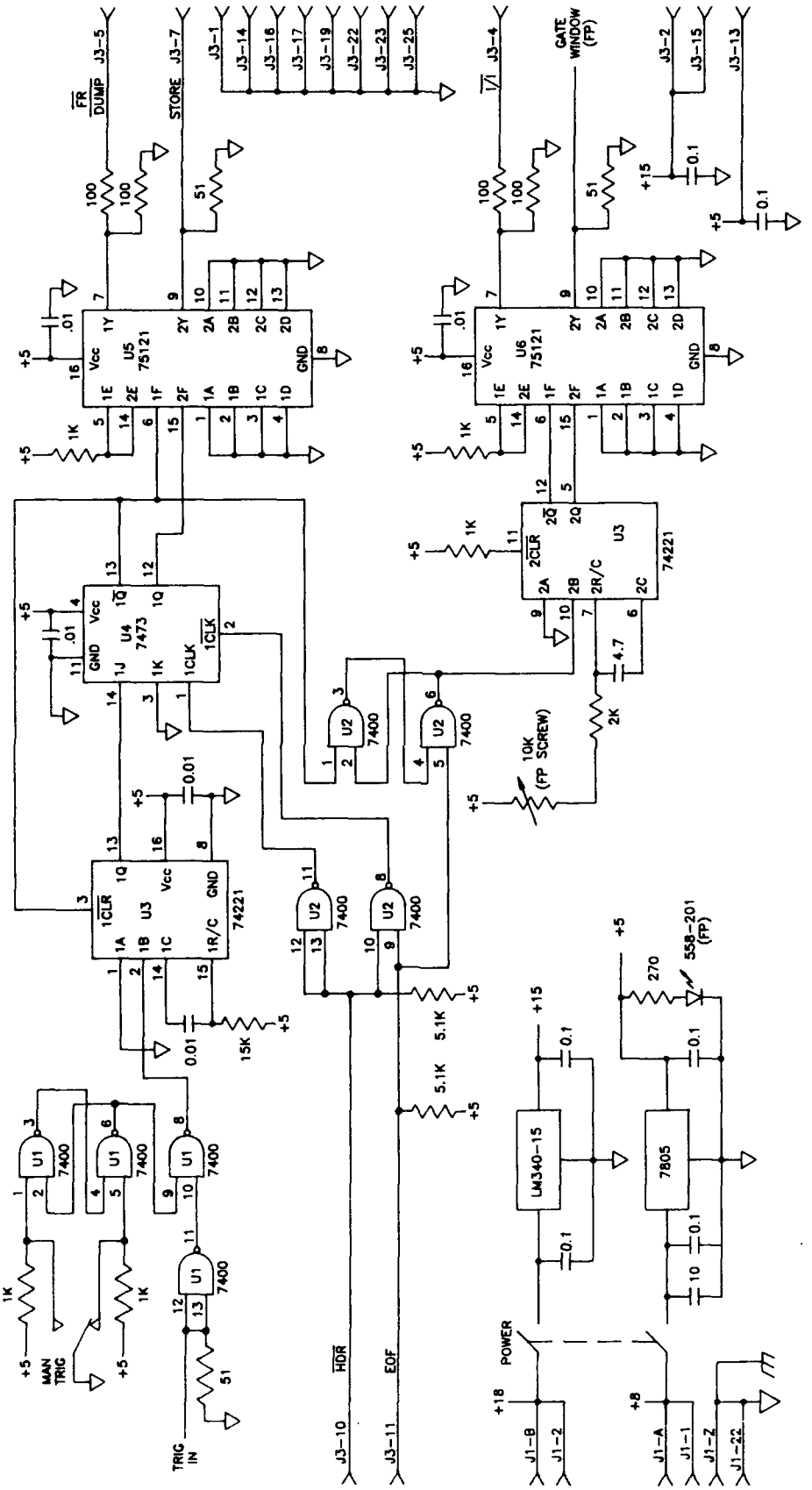

Figure 2-18. Electrical Schematic of Camera Control Module.

Section 3

THE 500-kV DIODE TEST FACILITY

3-1. GENERAL DESCRIPTION

Figure 3-1 is a block diagram of the major components of the 500-kV Diode Test Facility. The vacuum system and 500-kV pulse power supply are operational. Anode and cathode assemblies, however, were never constructed due to changing requirements and an eventual decision to terminate the effort due to budgetary constraints. Original plans were to pulse the anode with the positive output of the power supply and connect the cathode to earth ground (chamber potential). This would facilitate the operation of thermionic cathodes and gridded cathode systems. The design of the vacuum chamber and high-voltage bushing, however, also allows a grounded-anode, pulsed-cathode configuration.

The facility consists of 1) a 36-in-diameter, 43-in-long ultrahigh vacuum chamber, 2) a 250-nsec water-Blumlein pulse power source with selectable output voltage of 125 - 500 kV, 3) a low-inductance, variable-resistance load-matching resistor for dissipation of excess Blumlein energy, and 4) vacuum control and monitoring equipment, including a residual-gas analyzer, for maintaining and monitoring the vacuum environment. Provisions have been made for installation of the camera system, desktop processor, and electronic instrumentation (items presently installed in the 60-kV Diode Test Facility, see Section 2).

The separation distances required for accommodation of the 500-kV voltage peaks dictate that a number of system components be physically large. Other system requirements limit the choice of materials. These constraints result in the components being much too heavy for easy handling. Consequently, the structures have been separated into four major subassemblies which are mechanically independent of each other. Each subassembly includes grooved casters which match a floor-mounted V-rail system. The subassemblies can be separated for performing maintenance and reconnected without the need for realignment. In addition, each subassembly can be removed from the rail

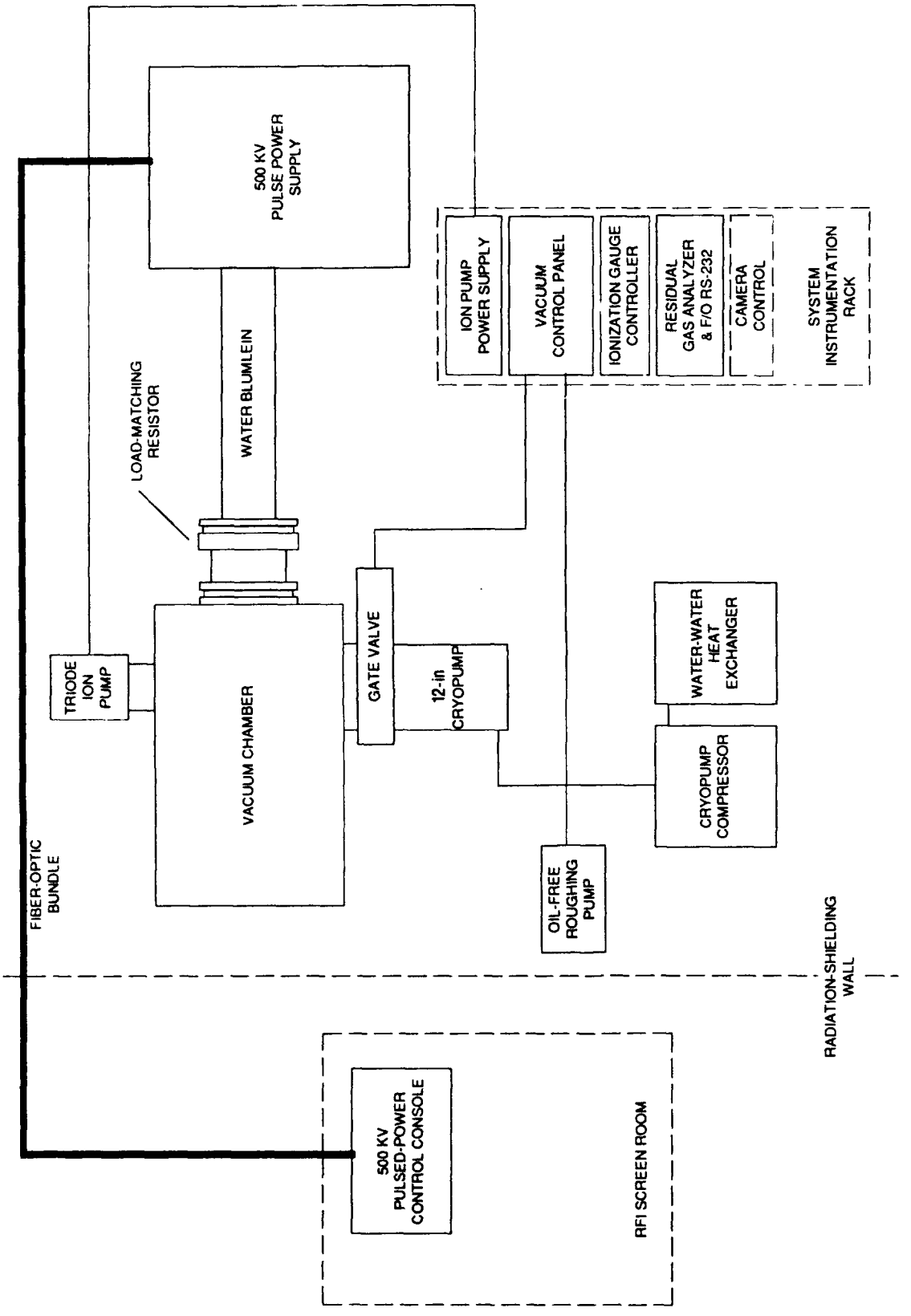

Figure 3-1. Block Diagram of 500-kV Diode Test Facility.

system and moved about the room with little effort. The subassembly breakdown is shown in Fig. 3-2. Figure 3-3 is a photograph of the system with the electrode mounting flanges attached to the vacuum chamber but separated from the power supply; the rail stand for the low-voltage electrode assembly is not shown in this photo.

Vacuum system monitors and controls are located in the System Instrumentation Rack (Fig. 3-1). The pulse power supply is controlled by a separate console, located within the RFI-shielding screen room and connected to the power-handling components via fiber-optic cables. The walls of the room housing the vacuum system and power supply are constructed of poured concrete with a minimum thickness of 24 inches which provides the necessary radiation shielding for high-voltage diode operation.

Since final anode and cathode configurations were never determined, the voltage and current monitors were not constructed. Conceptual designs, however, have been completed. Plans were to utilize a Rogowski-style[10] coil on the cathode assembly for current measurements and a water-capacitor voltage probe on the anode. Commercially available current and voltage probes are not compatible with the required high-vacuum environment, and accuracy would be seriously compromised if external probes were used.

3-2. A 500-kV DIODE VACUUM SYSTEM

The diode vacuum chamber is custom made; however, most of the other components of the vacuum system are commercially available. Figure 3-4 is a diagram of the chamber. The inside diameter is 36 inches and the length is 43 inches between the two wire-seal flanges. Stainless steel was used exclusively in chamber construction; the gaskets are OFHC copper. Clamp-type wire-seal flanges were used to facilitate angular alignment.

The system design calls for the anode-cathode gap to be aligned with the plane of ports nearest the 18-in wire-seal flange. This plane (designated the gap plane in Fig. 3-4) contains four 8-in vacuum-flange ports and four 4.5-in vacuum-flange ports, equally spaced around the outside of the chamber. These afford mechanical and optical access to the gap. A second plane of ports (four

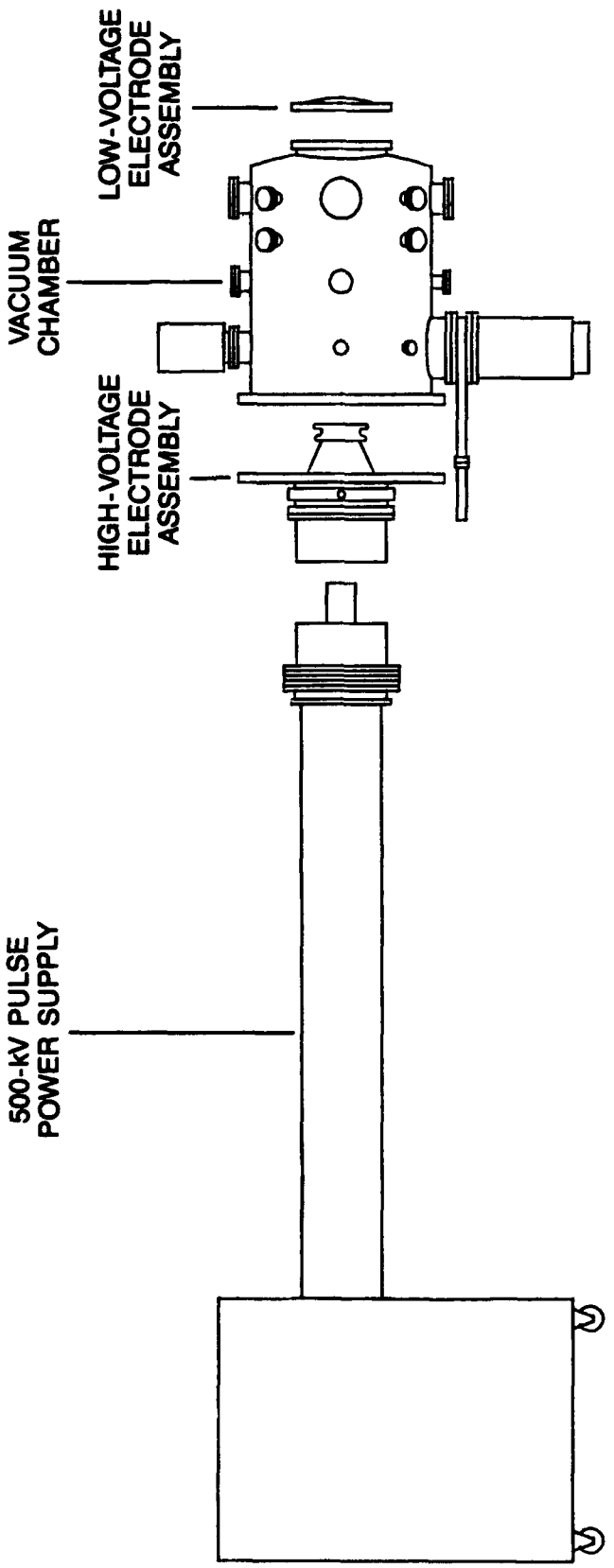

Figure 3-2. Diagram of Major Subassembly Breakdown of 500-kV Diode Assembly.

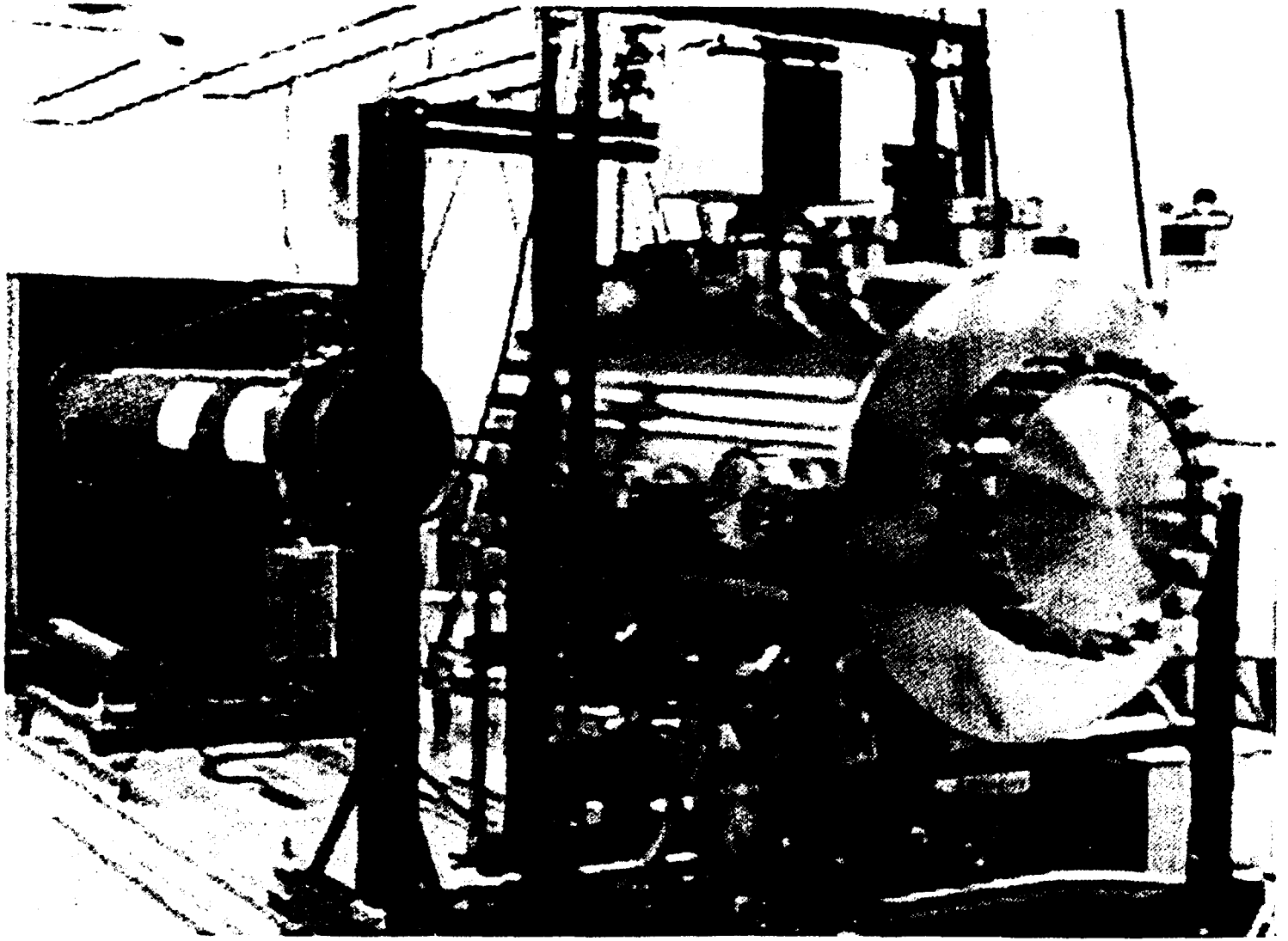

Figure 3-3. Photograph of 500-kV Diode Vacuum Chamber and Power Supply.

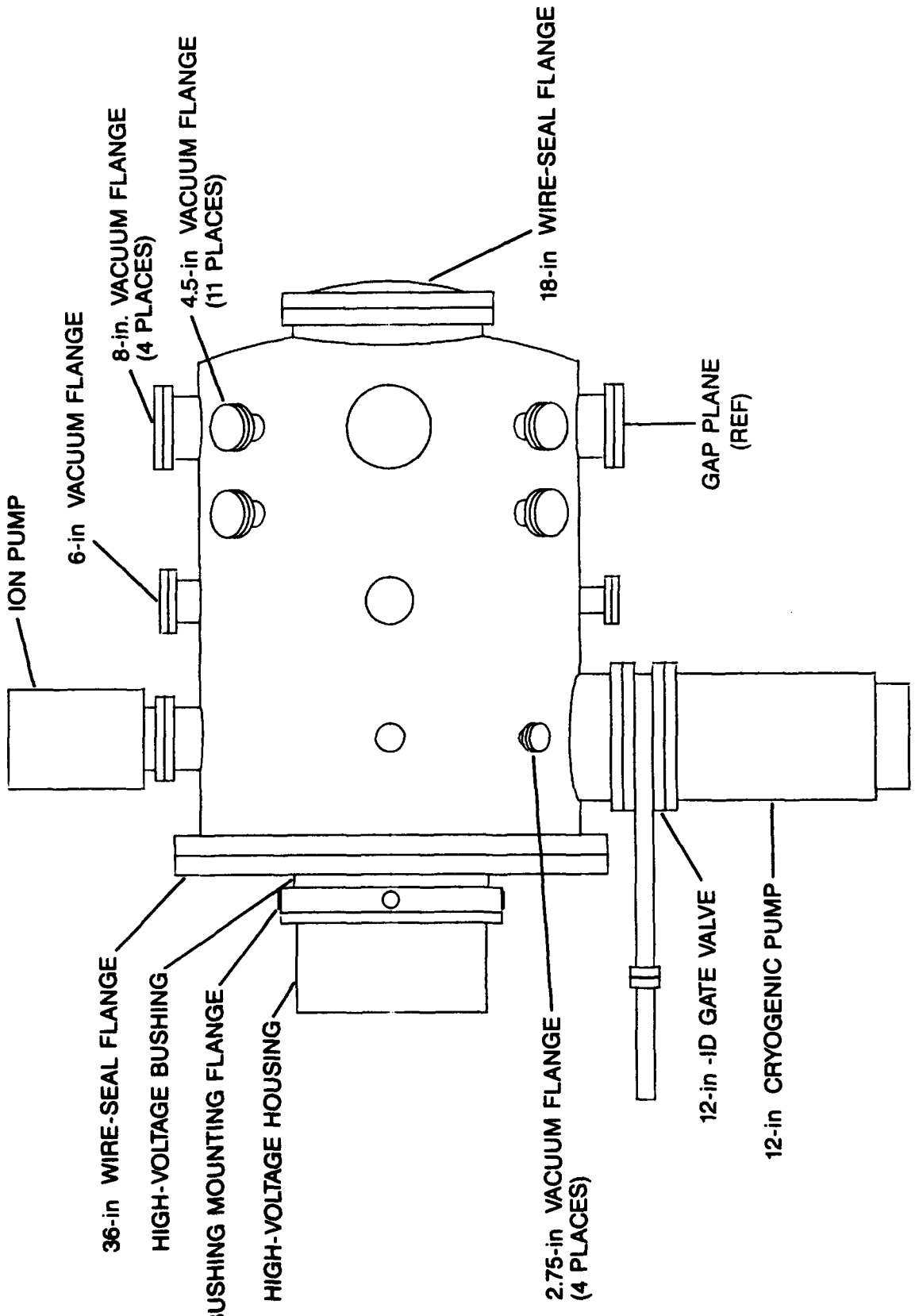

Figure 3-4. Diagram of 500-kV Diode Main Vacuum Chamber.

4.5-in flanges) is located a short distance from the gap plane, providing limited access to the gap and floating electrodes. A third plane of ports (three 4.5-in vacuum flanges and one 6-in flange) surrounds an area ~ 16 inches behind the floating electrode. This plane is intended to be used for diagnostics on the floating electrode, including a voltage probe and optical diagnostics such as a scintillator/camera arrangement similar to the current-density measurement apparatus presently installed in the 60-kV diode system (see Section 2). A fourth plane of vacuum ports is intended to be used for vacuum control and instrumentation and currently includes a 12-in cryopump, a 230-liter/sec ion pump, a nude ionization gauge, and a quadrupole residual-gas-analyzer head.

The 36-in wire-seal flange provides full access to the inside of the chamber. Although the flange is flat, the more than 2-in thickness of the 304 stainless steel is sufficient to prevent significant flexing as the chamber pressure is varied. This thickness also provides sufficient strength for support of the high-voltage vacuum feedthrough and the floating electrode assembly. A 22-in-diameter opening was machined into the wire-seal flange to accommodate the feedthrough. Maintenance on the feedthrough and floating electrode can be performed by removal of the feedthrough and assembly from the opening or by removal of the wire-seal clamps and separation of the chamber and flange, utilizing the V-groove caster system. The high-voltage, high-vacuum feedthrough (bushing) is discussed in more detail below.

The 18-in wire-seal flange is intended for mounting of the "grounded" electrode system. That is, the low-potential electrode is to be electrically connected to this flange which is directly connected to the chamber. Although a low-inductance shunt may be installed between the electrode and the flange, a Rogowski-style probe is the technique of choice for current monitoring because of the relatively high currents and fast risetimes expected. Figure 3-5 shows a suggested arrangement for mounting the low-voltage electrode. An e-beam-welded bellows provides vacuum isolation for the linear translation of the electrode system, and the ceramic spacer allows access of the Rogowski-style probe to the current-induced magnetic field of the electrode mounting tube. An approximately coaxial geometry and resulting low inductance are maintained within the extension as well as the 36-in-diameter chamber. Impedance mismatch presents only a minor problem because the length of the mismatched portion

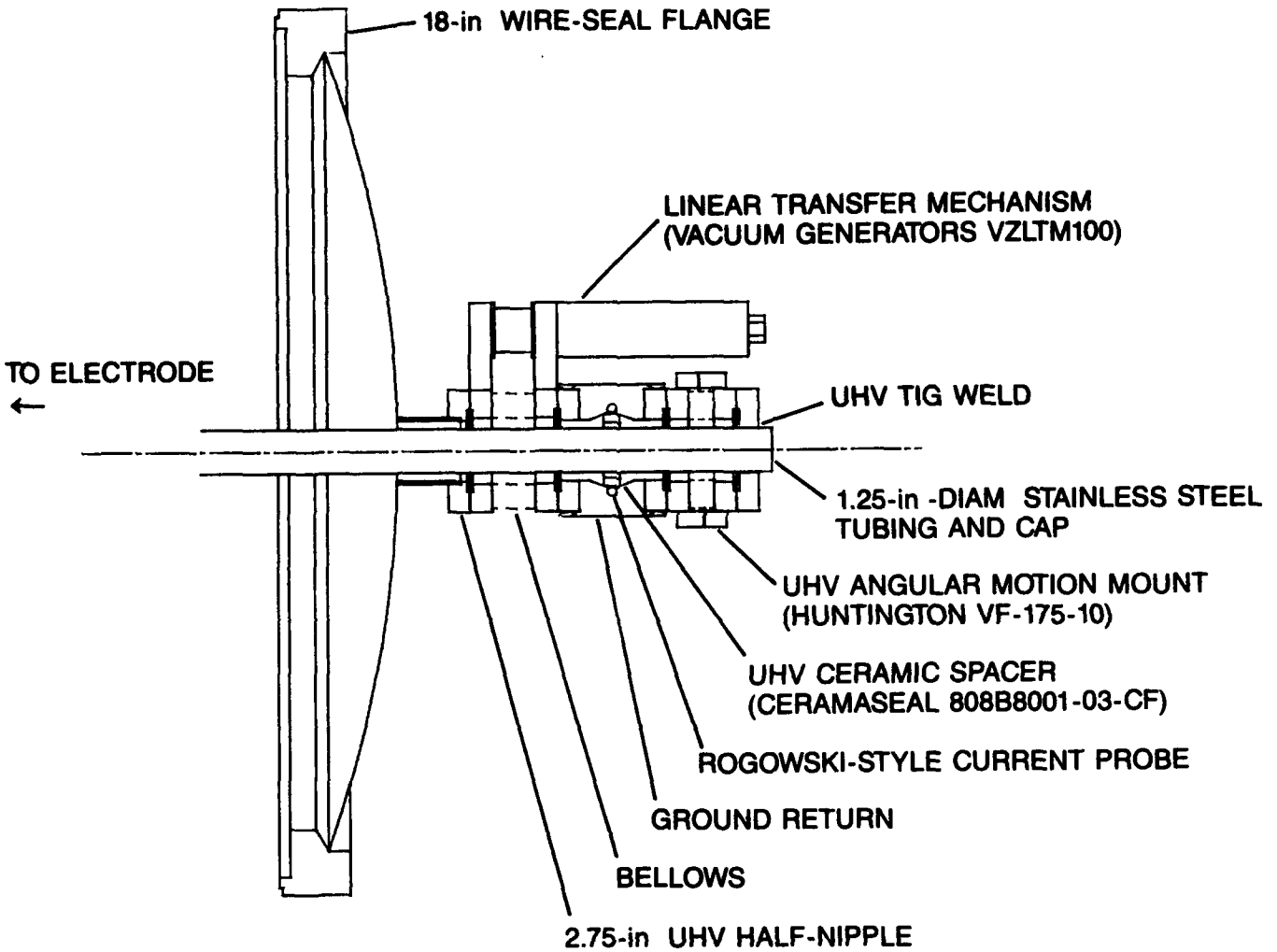

Figure 3-5. Conceptual Diagram of Cathode Mount for 500-kV Diode.

represents < 15 nsec (< 7.5 ft). The components shown in Fig. 3-5, with the exception of the mounting tube, are commercially available. The configuration of this tube will be dependent upon the type of electrode to be used.

3-3. A 500-kV VACUUM BUSHING

A 500-kV ultrahigh vacuum feedthrough (bushing) is not commercially available except on a custom basis. Only a few manufacturers possess both high-voltage and high-vacuum expertise. The high costs indicated by the few known suppliers of similar equipment precipitated a search for alternative materials and fabrication techniques. The major limitation was found to be the unavailability of large pieces (> 12 inches in diameter) of vacuum-compatible insulating materials.

One approach involved modifying commercial high-voltage bushings to make them vacuum-compatible. Such techniques as sealing the bushing material from the vacuum environment and modifying the material composition or manufacturing procedures were considered. The eventually successful approach involved a modification of the constituents of a 550-kV bushing manufactured by Westinghouse Corporation.[11] After initial consultation with personnel at the Massachusetts facility, a standard high-voltage bushing composed primarily of silica and alumina with aluminum inserts was supplied to us for testing.

A small high-vacuum test chamber was constructed using standard 2.5-in- and 1.5-in-diameter stainless-steel UHV plumbing. This chamber was then connected to the roughing port of the low-voltage diode cryopump through a 1.5-in-diameter gate valve. The result was a clean, high-vacuum system suitable for testing of small material samples. The lower pump port was used to minimize the potential of contaminating the gun chamber in the event of excessive outgassing from the test chamber. Although the pumping speed was restricted by the relatively small diameter of the vacuum plumbing and the location of the cryopump port, the speed was adequate for outgassing tests. Most importantly, the pump and system were oil free and bakeable.

The test procedure involved first thoroughly cleaning the empty test chamber and then vacuum baking to 200°C until the residual gas was at an acceptably

low background level. With the chamber at room temperature, the material sample was installed and pumped for 24 hours. The mass spectra were then recorded as the temperature was varied. A quadrupole residual gas analyzer (RGA) recorded the gas constituents. Total background pressure of the empty chamber was typically $< 10^{-7}$ Torr at room temperature and $< 10^{-6}$ Torr at 150°C.

Figure 3-6 shows representative mass spectra recorded at room temperature for the test chamber with and without a sample of the standard bushing material installed. These spectra were taken after several bake cycles (up to 150°C) to ensure that atmospheric and solvent residues were removed. Figure 3-6(a) indicates that outgassing of the chamber components (walls, valves, etc.) consisted primarily of a low level of water vapor (mass 18 and resulting H, H_2, O, and OH). Impurity lines are also seen at mass numbers 27, 43, 44, 94, 96, 129, and 131; but the total partial pressure of these was $< 2 \times 10^{-8}$ Torr. With the sample installed, the water content increased by an order of magnitude, as did the hydrocarbon impurities (indicated by mass 43). Several other impurities also increased.

The disturbing characteristics of the sample, however, were the continual excessive outgassing at elevated temperatures and the failure to reduce the source of water vapor by baking. After 4 days of baking at 150°C (7 - 8 hours/day), the room-temperature pressure was 5.5×10^{-5} Torr which represents only a 30% reduction in outgassing rate. In contrast, the reduction in pressure of an empty chamber under similar conditions was 3 orders of magnitude.

In addition, pressure bursts were observed as the temperature was varied. As shown in Fig. 3-7, a jump in pressure was observed as the temperature decreased. This jump consisted primarily of water vapor although several other impurities were also recorded. The amplitude of masses 36 - 41 and 49 upward decreased with temperature--the expected behavior of clean vacuum systems. The fact that the pressures associated with the remaining mass numbers increased with decreasing temperature seemed to indicate that some physical change had occurred in the sample. A leak to the atmosphere was ruled out because little change in O_2 amplitude was observed and a leak check using He

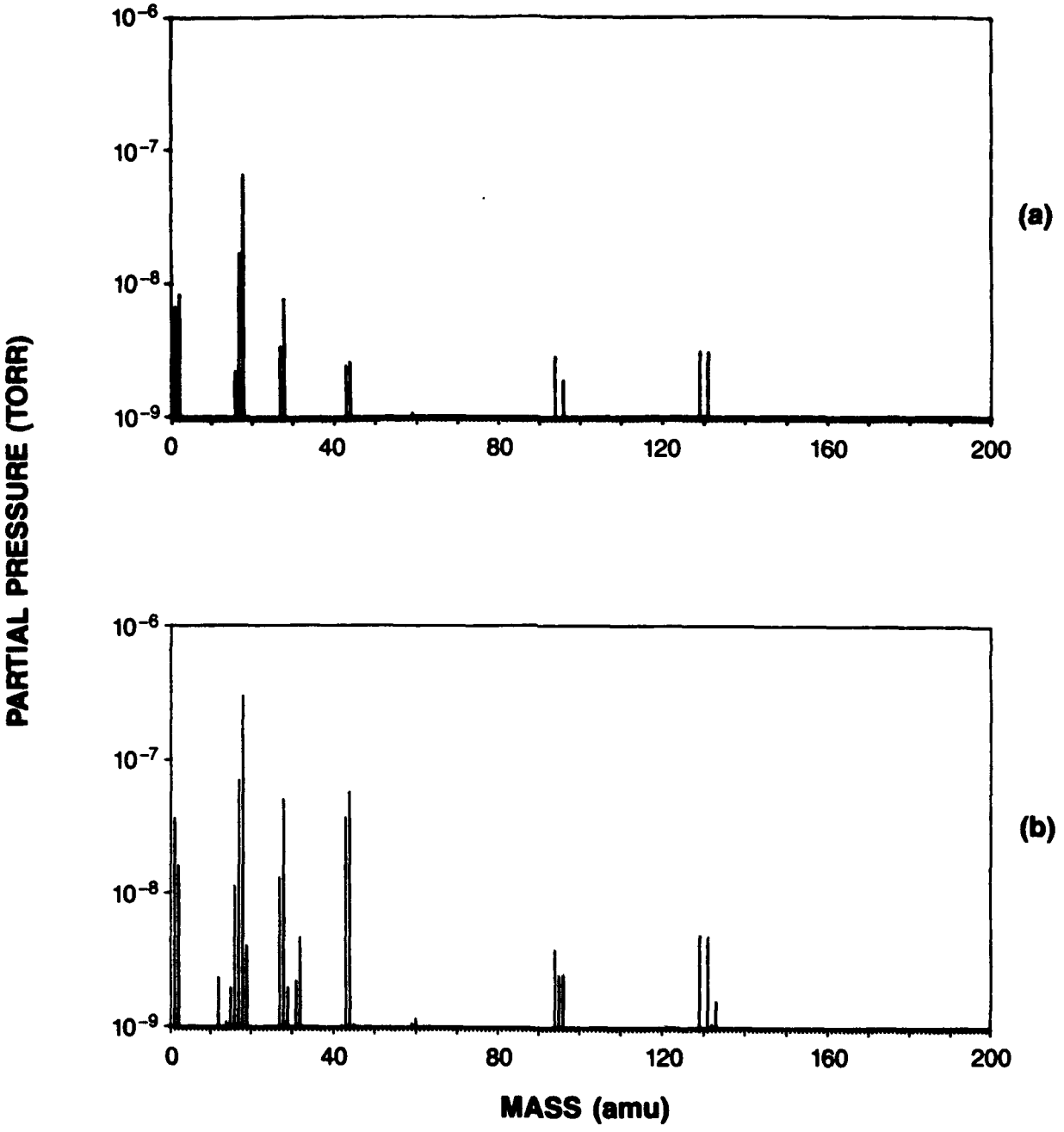

Figure 3-6. Mass Spectra of (a) Empty Test Chamber and (b) Test Chamber with Sample Installed.

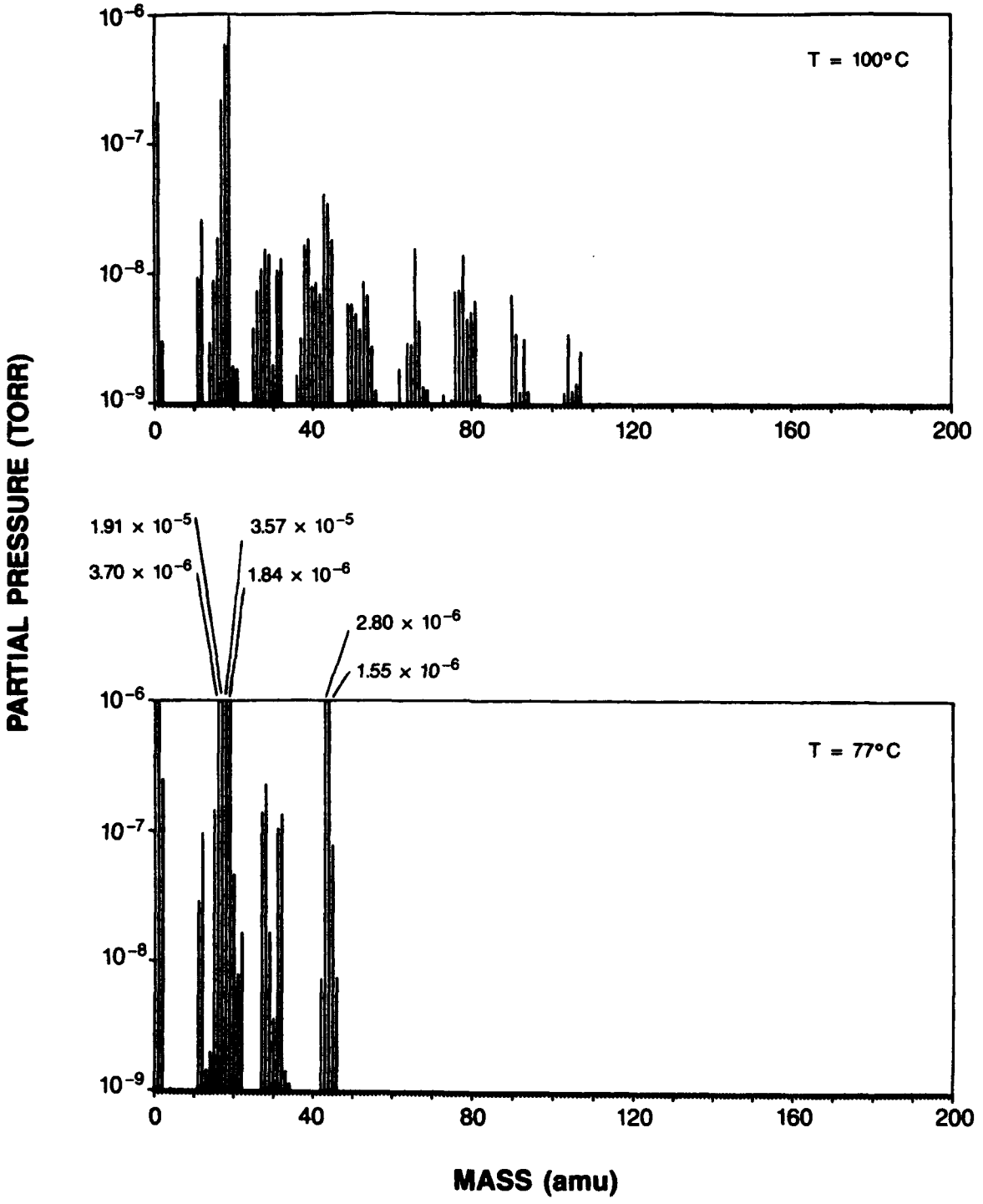

Figure 3-7. Mass Spectra of Test Chamber with Sample Installed as Temperature is Decreased.

indicated no leak. Probably some fissures appeared as the temperature changed, causing a release of trapped gases from the sample.

In addition to water, the impurities which increased at the pressure burst included carbon (C but not C_2) and remnants of simple hydrocarbons which probably resulted from manufacturing and/or cleaning processes. The presence of SiH_4 is also indicated (by masses 29 - 34) and may result from a significant portion of the material composition being silica, although the partial pressure of $> 10^{-7}$ Torr is surprisingly high. Lines at masses 11 and 19 are particularly perplexing. According to the manufacturer, the composition contains no boron or fluorine, nor did the manufacturing process introduce these elements. Although acetone causes a peak in mass spectra at 19, it also causes a significant peak at mass 58; however, no evidence of mass 58 is observed for the 3 orders of magnitude of Fig. 3-7. The most plausible explanation is that cleaning solutions had been absorbed into pits and fissures on the sample and aluminum surfaces. The history of the test bushing is, for the most part, unknown although Dynasoap 105S (Heat Systems-Ultrasonics Inc.), trichloroethylene, methanol, and acetone were used in cleaning operations.

Consultation with the manufacturer led to the suspicion that the source of the water is a hydrated form of one of the compounds used in the mixture. If this were the case, it would be unlikely that the outgassing could ever be reduced to an acceptable level. However, an unhydrated form of the compound was supplied to the manufacturer, and a small sample bushing was cast.

Vacuum-compatibility tests of the modified compound showed marked improvement in the vacuum characteristics. After 2 weeks in a vacuum environment, including seven heating cycles to 120°C, the sample exhibited no measurable outgassing. The ultimate pressure measured with and without the sample installed was 2×10^{-9} Torr. The only contaminants observed were traces of N, N_2, CO_2, CO, and water residuals (H, H_2, O, O_2, OH, and H_2O). The very low levels, however, made measurements with the present RGA unreliable. A more practical indication of ultrahigh vacuum compatibility is the leakup rate, i.e., the rate of increase in pressure due to outgassing measured with the pumps closed off. A leakup rate of $< 10^{-8}$ Torr liter/sec was measured with the sample installed. Although this rate may vary with the chamber pumping and

baking history, little difference was observed between leakup rates measured with and without the sample installed. Therefore, it was concluded that the altered bushing-material composition is compatible with the cleanliness requirements of the e-beam diode vacuum system; several bushings were then cast.

A diagram of the bushing is shown in Fig. 3-8 along with the stainless-steel cap. This cap serves two main purposes: 1) it isolates the aluminum center conductor of the bushing from the vacuum environment (a Viton[12] o-ring facilitates the seal), and 2) its shape helps prevent the formation of surface arcing at the insulator/conductor interface (typically referred to as the triple-point). The cap also serves as the mounting platform for the floating-electrode assembly.

Viton o-rings are used for vacuum sealing to the insulator material. Minor difficulty was encountered in obtaining an acceptable seal, presumably due to the microscopically rough texture of the material. However, use of a slightly larger cross section than that specified by normal design guidelines alleviated this problem.

The main limitation imposed by the use of the cast alumina/silica compound is the inability of the material to withstand a high-temperature vacuum bakeout. According to the manufacturer, the material begins to soften at 150°C. The large size of the bushing means that high force is present across the bushing when the chamber is under vacuum. Therefore, no softening or other weakening of the bushing can be tolerated; the recommended temperature limitation is 120°C. Although this temperature would be helpful for removal of adsorbed water and volatile compounds, an extended low-temperature vacuum bakeout may be necessary for attainment of ultrahigh vacuum. In operations to date, however, pressures < 10^{-8} Torr have been reached in the vacuum chamber without elevating the temperature above 22°C.

3-4. A 500-kV PULSE POWER SOURCE AND LOAD-MATCHING RESISTOR

The 500-kV pulse power supply was manufactured by Impulse Engineering.[13] It is a pulse-charged, spark-gap-switched, coaxial water-Blumlein capable of operation at voltages up to 500 kV and supplying up to 6 kJ of energy in a

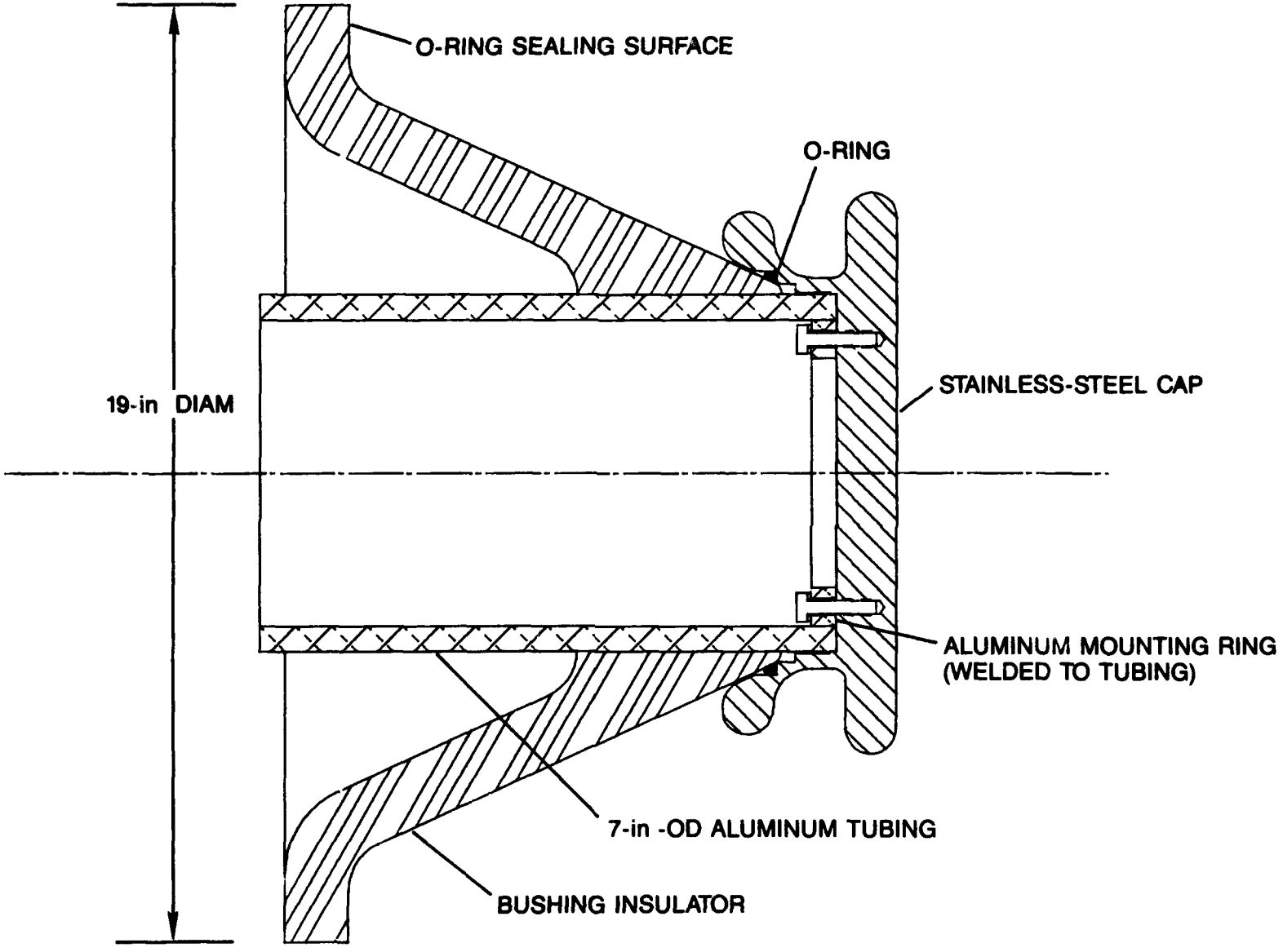

Figure 3-8. Cross-Sectional Diagram of 500-kV Vacuum Bushing with Cap Installed.

250-nsec (FWHM) trapezoidal-shaped pulse. The operating characteristics of a Blumlein dictate that the pulser load be "matched" to the characteristics of the transmission lines of the pulser. That is, if the load dissipates power at a rate differing from the designed delivery rate of the lines, a portion of the line energy will be reflected back and will reappear at the output at a later time. Obtaining the proper load-dissipation rate is generally referred to as impedance matching.

Since the impedance of the vacuum diode may vary by several orders of magnitude, depending upon such factors as gap voltage, gap spacing, and cathode emission characteristics, some method of providing the power supply with a matched impedance must be found. For this purpose a disc-shaped, liquid resistor was mounted directly onto the power supply and in parallel with the output and the diode gap. The disc shape helps to maintain a low inductance, and the $CuSO_4$/water solution provides sufficient heat capacity for the large pulse energies available.

Although solid resistors were previously considered to be more desirable than the liquid type, consultations with resistor manufacturers and others in the field have indicated that the solid materials available could not withstand the very high peak currents needed. That is, the specified maximum current densities of available materials would be exceeded by more than a factor of 2 (at maximum pulser output). Furthermore, the physical mounting requirements of the solid resistors as well as their relative inflexibility with regard to changing resistance values resulted in liquid resistors becoming the most attractive option. Also, the time response of a $CuSO_4$ resistor was measured and found to be acceptable for the expected pulse risetimes of > 20 nsec.

Figure 3-9 is a cross-sectional view of the disc-resistor construction. Essentially, the unit is a 1-in-thick disc resistor made up of copper-sulphate resistive solution ($CuSO_4+H_2O$) sandwiched between two acrylic plates. The pulser output--center conductor of the Blumlein--is connected to a 5-in-diameter copper disc via threaded rod. A 16-in-ID, 23-in-OD copper ring constitutes the ground termination of the resistor; a copper sheet with beryllium-copper contact fingers (not shown) connects the ring (outer electrode) to the "ground" potential of the Blumlein mounting flange and the cylindrical aluminum housing. That is, the path of the load current is between the inner disc and outer ring. The diode load

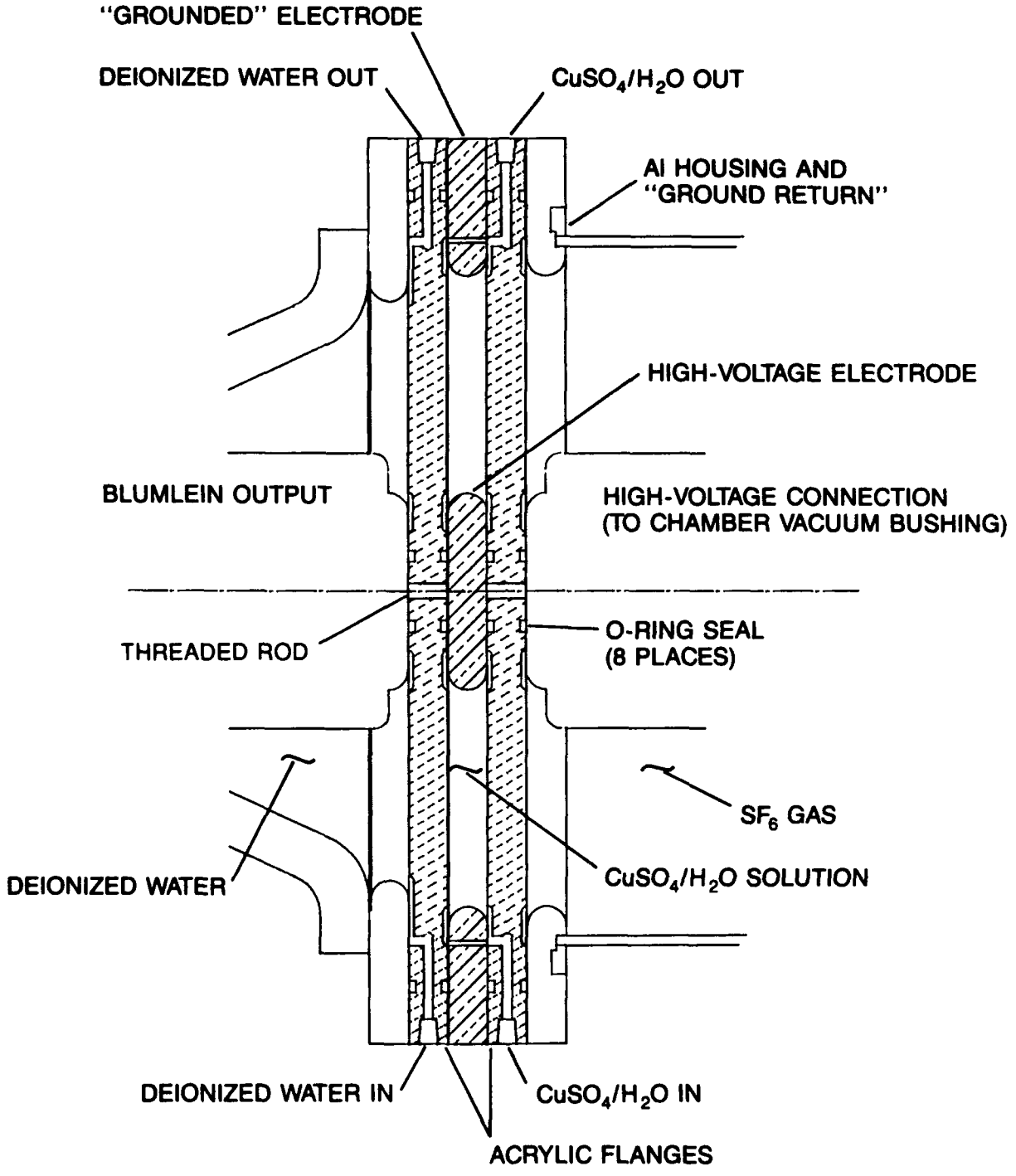

Figure 3-9. Cross-Sectional Diagram of 500-kV Copper-Sulphate Disc Resistor.

is also connected to the center conductor. In this manner, the $CuSO_4$ resistor and diode are in parallel. Ideally, the parallel combination of the two loads would represent a matched impedance to the Blumlein.

The main advantages of the load-resistor arrangement are the low inductance and the ease with which the resistance value can be changed. Also, since the resistor is primarily water, high voltages and high energies can be safely accommodated. The main disadvantage of liquid resistors is the increased complexity resulting from the mixing and handling of a liquid which is often corrosive. For the present arrangement, Cu electrodes were used in order to minimize electrode effects. Also, chemically inert materials were utilized throughout the liquid-handling system.

A small aquarium-style pump and reservoir were included in the system to provide a continuous flow and facilitate mixing. The resistance of the solution can be varied with little effort by adjusting the proportion of a saturated $CuSO_4$/water mixture and deionized water. The resistance of the disc resistor is continually displayed by a unique pulsed monitor inserted in the liquid line just upstream of the resistor.

A schematic diagram of the resistance monitor is shown in Fig. 3-10. The circuit is essentially a sample-and-hold circuit synchronized to a pulsed 1-μsec, 10-mA current source. The "resistor" is a 0.75-in-diameter, ~ 1-in-long chamber inserted into the liquid line immediately upstream of the large disc resistor. Scaling circuits cause the digital display to indicate the approximate ohmage value of the disc resistor. Presently, the displayed resistance value is only approximate; the shape of the high-voltage pulse is used as the final determination of the suitability of the solution resistivity. A more accurate display can be obtained, however, by calibration of the circuit against an accurate pulse monitor connected to the disc resistor after removal from the Blumlein.

The 500-kV pulse power supply is not operational at this time. Two situations must be changed before the system can be used. First, a defective thyratron tube (EEV CX1622) must be replaced; this tube is one of the six arranged in parallel which constitute the resonant charge switch. Second, the timing of the thyratron and spark-gap trigger must be adjusted to accommodate the

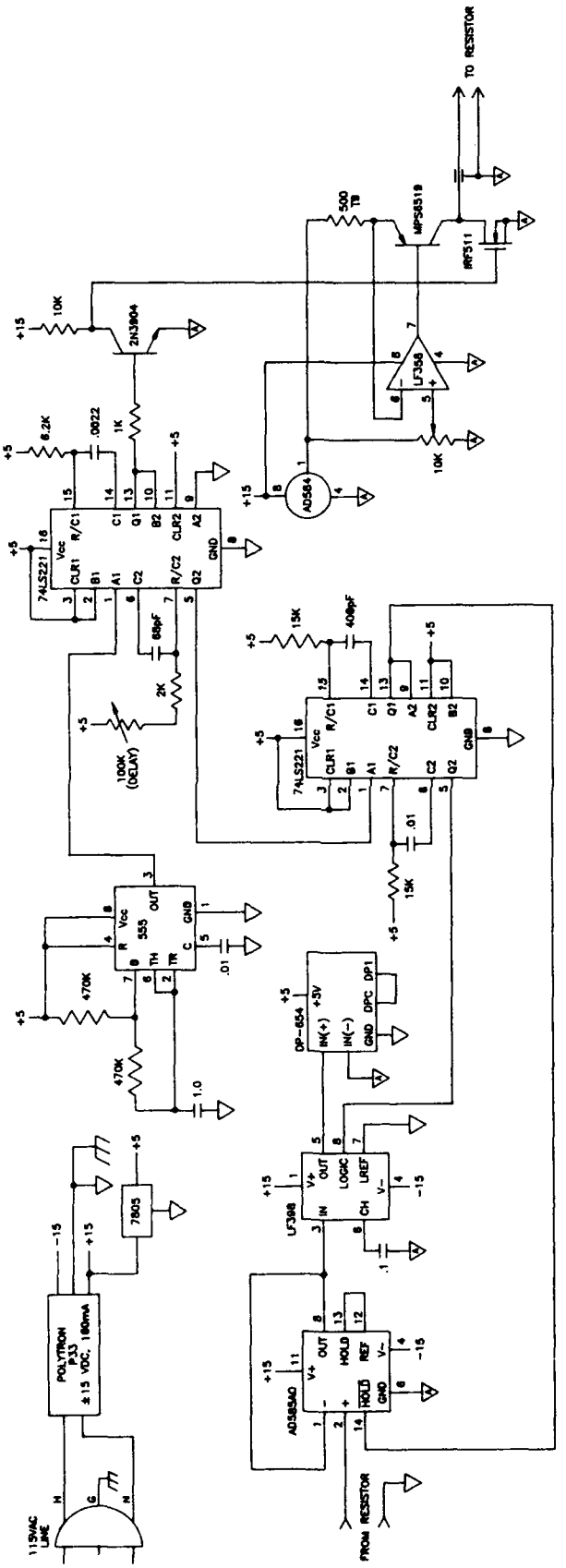

Figure 3-10. Electrical Schematic of Pulsed Resistance Monitor.

reconfiguration of the Blumlein, i.e., when the 3-Ω/6.7-Ω Blumlein arrangement was changed to the 3-Ω/3-Ω symmetric configuration, the capacitance of the line increased sufficiently that the original synchronization timing was no longer correct. However, the loss of the thyratron precluded adjustment at the time of the reconfiguration.

It is recommended that the symmetric configuration of the Blumlein line be maintained. Because of the operating characteristics of a Blumlein, reflections at the output will occur unless both transmission lines which constitute the Blumlein arrangement are of equal length and impedance and the load impedance is equal to the sum of the two lines. To date, the system has been successfully operated only with the unsymmetrical 3-Ω/6.7-Ω arrangement. Operation without reflections was not possible, although adjustment of the matching resistor to ~ 38 Ω resulted in a pulse shape having a 115-nsec rise-time, a 144-nsec flat (< 5% variation) top, and a 100-nsec fall time. The relatively high load impedance was needed to obtain the proper voltage level and prevent overshoot and undershoot. Subsequent reflections contained < 25% of the energy of each previous pulse. That is, adjustment of the load impedance for the most ideal pulse shape resulted in a string of pulses separated by the Blumlein line length, with each successive pulse having an amplitude less than one-half that of the previous pulse. The manufacturer's operating and service manuals should be consulted for more details.

3-5. PULSE CURRENT AND VOLTAGE MONITORS

As mentioned previously, the current and voltage monitors must be built *in situ* because of the demanding requirements of measuring high-speed, high-voltage pulses within a high-vacuum environment. Since the final configurations for anode and cathode mounts were never determined, the monitor designs were not completed. However, detailed conceptual designs were formulated.

The pulsed current measurements are expected to be relatively straightforward. A Rogowski-style coil can be commercially manufactured to approximately encircle the ceramic spacer shown in Fig. 3-5. For high accuracies at fast rise-times, it may be necessary to compensate for the finite frequency response of

commercial probes, but the current signal is typically recorded as a digitized waveform which can be readily corrected within the system processor.

In contrast to the current monitor, no suitable voltage monitor is available commercially. Although sophisticated techniques such as fiber-optic and Kerr-effect electric-field sensors were considered, a capacitive-divider scheme is much simpler, more reliable, and easier to construct within a high-voltage, high-vacuum environment. Although the high voltage limits the choice of suitable dielectrics, a recirculating deionized-water supply is readily available since water is the dielectric medium of the power-supply Blumlein. Therefore, a water-dielectric capacitive divider is the technique of choice.

Figure 3-11 shows the recommended voltage-divider design. The parts are commercially available except for the glass tubing, the divider disc, and the divider/amplifier electronics. The electronics, however, may be the same (with the exception of the low-voltage capacitor) as those used in the 60-kV capacitive divider of Section 2 (shown in Fig. 2-16). The divider disc may be readily machined from stainless-steel stock or other suitable conductive material (aluminum and copper are not recommended for long-term use in water). Although the glass tubing (26- to 35-mm-OD Pyrex) can be purchased, the availability of glass-to-metal transitions will determine the practical diameter. Figure 3-11 is a scale drawing using 35-mm tubing. Utilizing the dimensions represented in Fig. 3-11, the capacitance of the high-voltage leg is calculated to be ~ 1 pF which is suitable for use, provided the leakage current at the input of the divider/amplifier circuit is not too large.

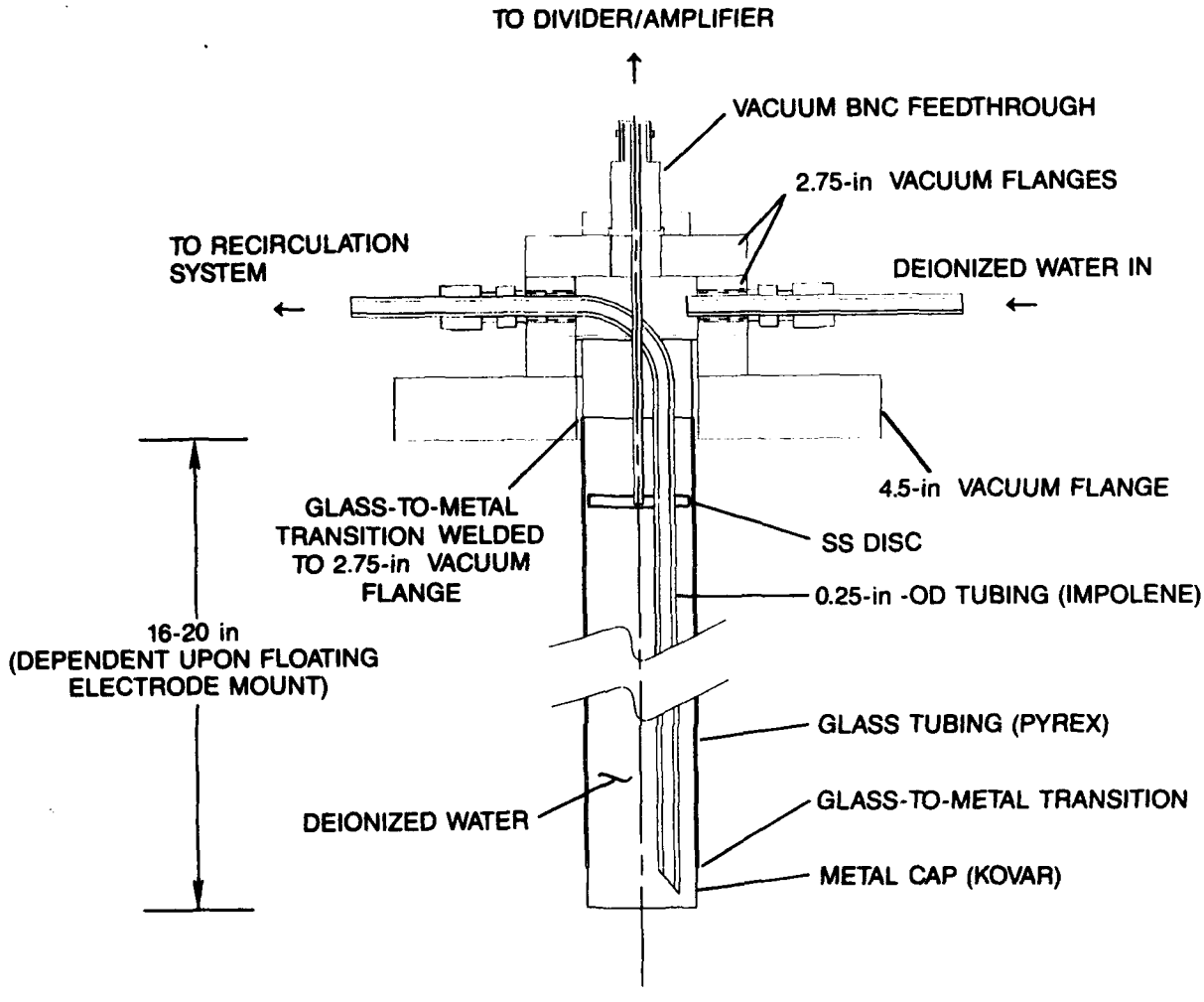

Figure 3-11. Conceptual Design of High-Vacuum 500-kV Capacitive Voltage Divider.

Section 4

PHOTOCATHODE MEASUREMENTS

As a result of renewed interest in photocathode operation,[2-4] the low-voltage diode was reconfigured for operation with a photocathode, and conceptual designs for modification of the high-voltage diode system were formulated. Shortly after the initiation of preliminary measurements, however, the effort was terminated due to budgetary constraints. The discussion here briefly summarizes the planned approach.

Figure 4-1 shows the optical arrangement for wavelength-threshold and photoelectron-yield measurements. A Xe light source and 1/4-m scanning monochromator constitute the narrow-band source. The output of the monochromator passes through a Suprasil lens and a sapphire window into the vacuum system and is directed through a hole in the anode foil to the cathode by a UV front-surface mirror. The wavelength-selective light also passes through the BaF_2 scintillator (used for physical support in this case) and a mask. This mask minimizes photoemission from the molybdenum anode.

For calibration, the cathode is replaced with a UDT Sensors, Inc., silicon photodiode calibrated in the wavelength range 200 - 1100 nm. Calibration of this detector is traceable to NBS and was utilized to determine the absolute intensity of the light reaching the cathode surface. Figure 4-2 shows the measured optical intensity utilizing the available monochromator grating and optics which were most sensitive to the ultraviolet spectral region. No correction was made for the ~ 1-nm linewidth of the monochromator since the change of intensity as a function of source wavelength was relatively gradual. The maximum error caused by this is estimated to be < 2.5% and primarily causes an understatement of the photon yield in the vicinity of the cutoff wavelength of a photocathode.

The setup in Fig. 4-1 was to be used for evaluation of photoelectric yield and wavelength characteristics of selected materials. For the present purposes, the yield is defined as the number of electrons emitted per incident photon. The

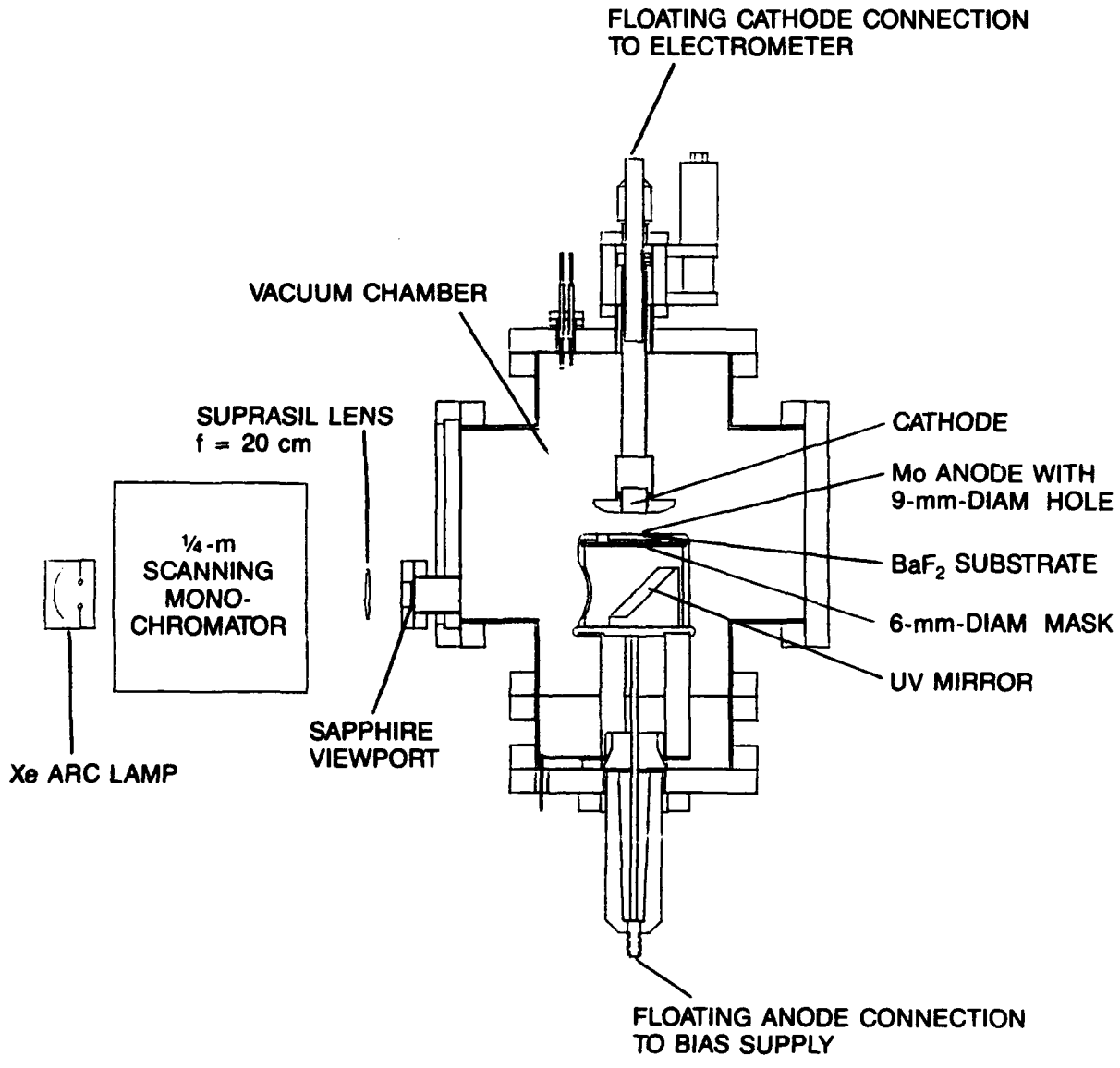

Figure 4-1. Cutaway View of Optical Setup Used for Photoemission Measurements.

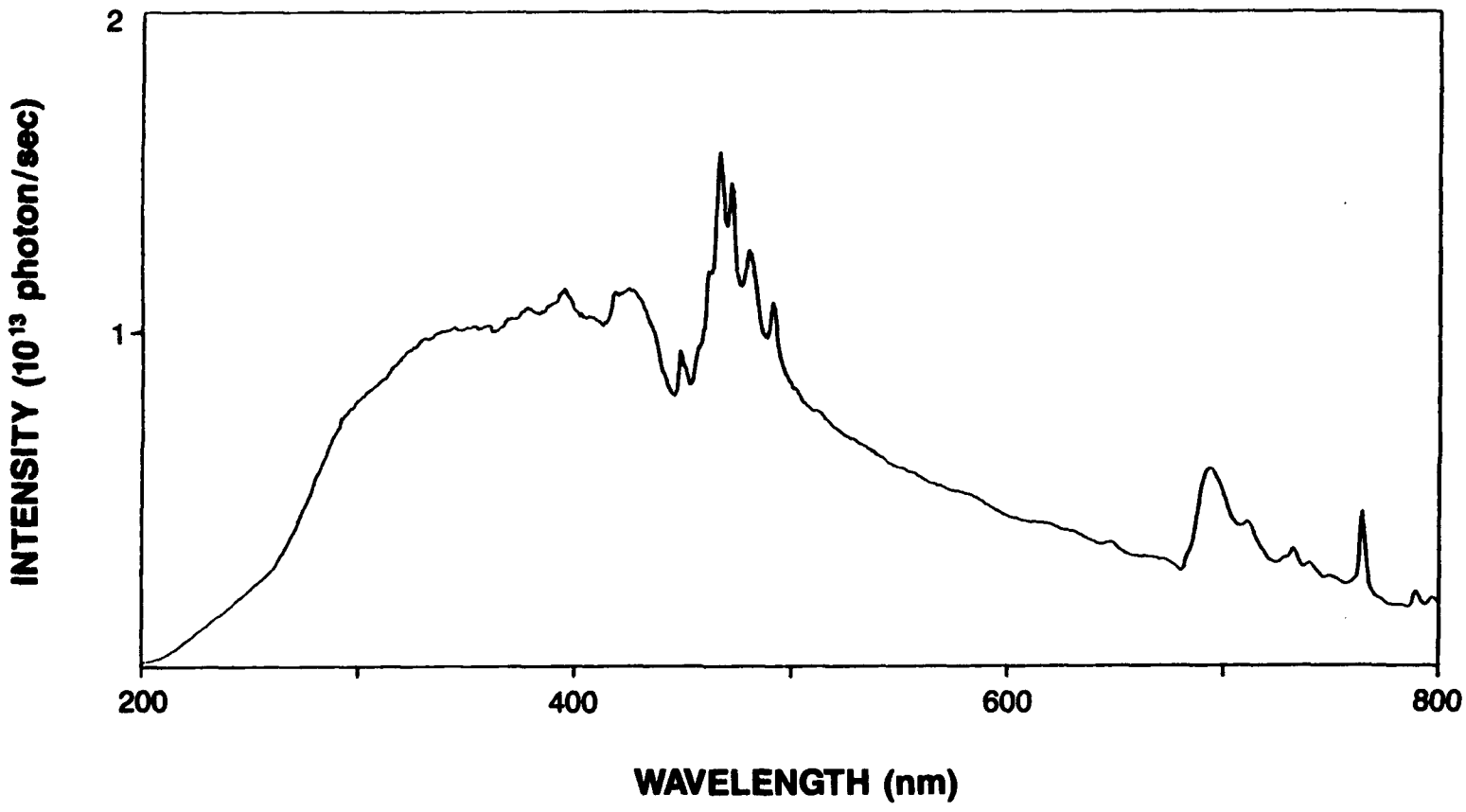

Figure 4-2. Optical Intensity of Light Source Measured at Cathode Position.

apparatus did not possess the capability to determine the absorption or reflection characteristics.

Although it is desirable to determine the "work function" of a photocathode, this term is often misused. That is, the work function is generally considered to be the minimum energy of a photon which results in emission of an electron. Unfortunately, the start of photoemission as a function of wavelength is generally not an abrupt transition, except possibly at zero degrees Kelvin. Also, the physical process of photoemission is different for a metal and a semiconductor.

Within a metal, the energy of the readily available conduction electrons is governed rather well by Fermi-Dirac[14-16] statistics; therefore, photon emission can be described mathematically by modification of the statistical electron-energy-distribution function. That is, the process is essentially photoexcitation of a free electron (free-free transition). Fowler[14] combined Fermi-Dirac statistics with the assumption that the number of emitted electrons is proportional to the number of electrons with sufficient energy in the direction perpendicular to the surface to penetrate the surface barrier after addition of a quanta of photon energy and redistribution by electron-electron collision. This approach did not fit experimental data. However, modification of the assumption for immediate ejection of a photoelectron (before the occurrence of energy redistribution) yielded excellent agreement with experimental data. That is, the successful assumption was that the number of ejected electrons is proportional to the number of electrons which, when augmented by a quanta of optical energy, have sufficient energy in the direction perpendicular to the surface to escape.

As a result of Fowler's work, a fit of the Fowler function to experimental data will yield a temperature-independent photoelectric threshhold for a metal. This threshhold may be considered the photoelectric work function and is related to the thermionic work function. Since Fowler's method does not require extrapolation of an asymptotically approaching value, it is much more desirable than mere extrapolation of photocurrent-vs.-wavelength data.

In contrast to photoemission of a metal, that of a semiconductor arises from the photon energy being used to move an electron from the valence band into the conduction band (bound-free transition) with sufficient excess kinetic energy to

overcome the surface barrier.[16-17] Formulation of a universal mathematical model for semiconductors is not possible because 1) photons are absorbed into energy levels which are quantized and cannot be described by a continuous statistical function, 2) the statistical distribution of valence band levels is strongly influenced by impurities within the semiconductor, 3) each semiconductor material has different valence-level to conduction-level (band gap) energies and vacuum-level (electron affinity) energies, and 4) photons generally penetrate a significant distance into a semiconductor; therefore, photoelectron scattering (both elastic and inelastic) must also be considered.

Determination of a semiconductor photoemission threshhold is generally limited to extrapolation of photocurrent-vs.-wavelength data. A Fowler function will typically not be a good fit to the data. The inability of the Fowler function to fit the data is considered an indication of a semiconductor photoemitter rather than a metal. That is, although the photocathode bulk may be a pure metal, the actual emitting surface may be a semiconducting metal oxide.

The results of preliminary photoelectric measurements of a barium-oxide dispenser cathode are shown in Fig. 4-3. The experimental data were collected at three different times: 1) as the cathode was being heated, 2) ~ 1 hour after the heat had been removed, and 3) ~ 3 hours after the heat had been removed. Fowler-function fits yielded only general agreement. The main point demonstrated by the data is the change in wavelength threshold with cathode "aging." That is, the photoelectric work function increased by over 30%, even though it was maintained within a UHV environment (< 10^{-8}-Torr pressure). This phenomenon is repeatable and has been observed previously.[18]

The measurement results of Fig. 4-3 are only preliminary. The slope of the data is biased by an estimate of the current-offset value made necessary by the very low currents observed. Refinement efforts were discontinued when the work was terminated.

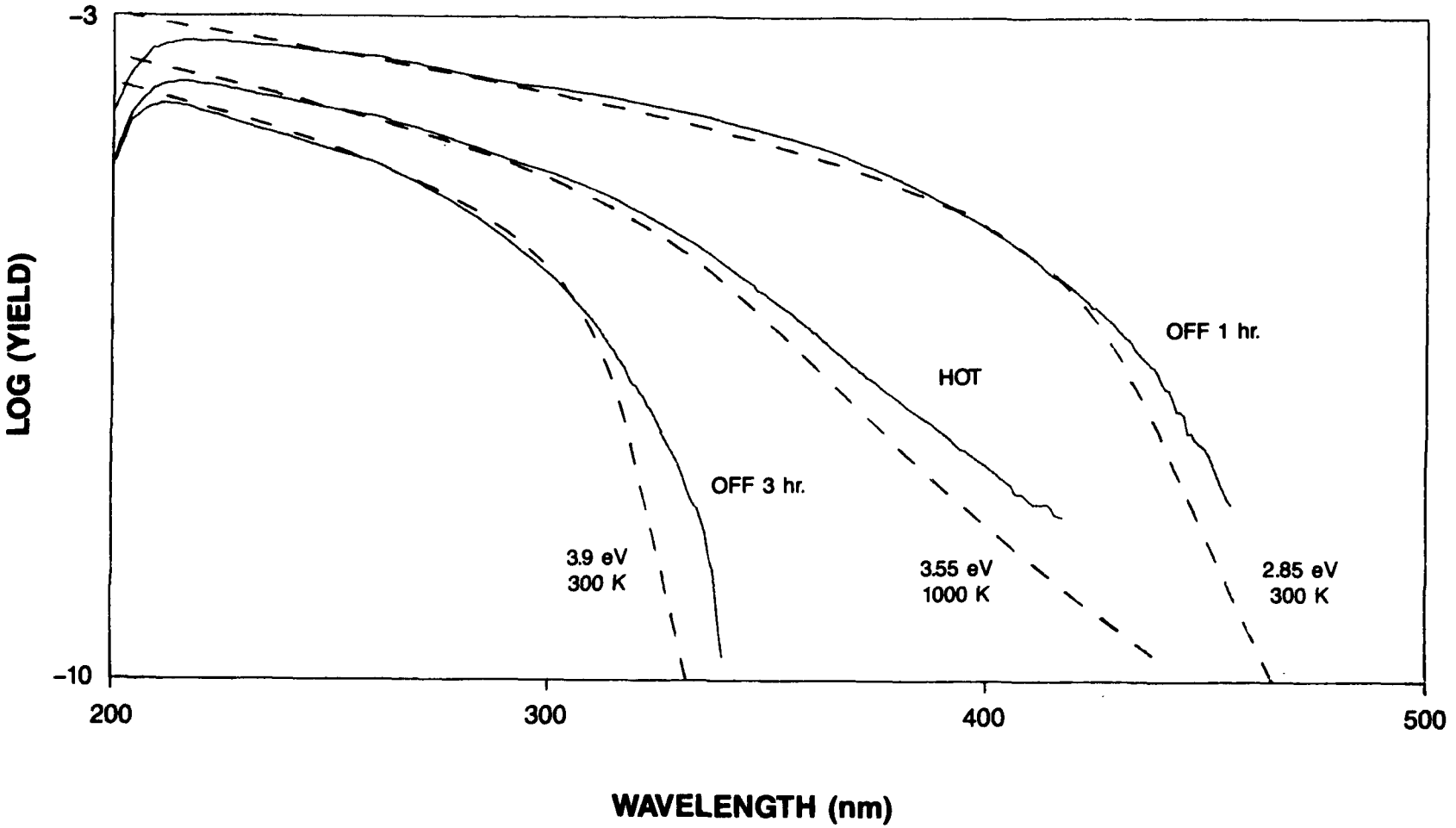

Figure 4-3. Fowler Fits for Determination of Photoelectric Work Function of BaO_2 Cathode.

Section 5

CONCLUSION

Two vacuum-diode facilities have been constructed at Wright Laboratory, Aero Propulsion and Power Directorate, Wright-Patterson Air Force Base, Ohio. One facility has been operated in a pulsed-anode configuration at voltages up to 80 kV with a 1-in-diameter beam. The facility is relatively small, simple to operate, and, in most applications, relatively easy to modify for accommodating changing experimental requirements. The diode chamber and all instrumentation within it are designed and constructed for extremely low outgassing, greatly minimizing the influence of environmental contaminants on diode operation.

The second facility was designed and constructed for a 5-in-diameter beam in pulsed operation at voltages up to 500 kV. As part of the design effort, an inexpensive high-vacuum, high-voltage bushing was developed. The large vacuum system and the pulse power supply have been checked out, but no anode or cathode has yet been installed. The high voltage allows a much higher beam current and larger gap spacing than possible in the low-voltage facility, but components having large physical sizes are required to prevent undesired high-voltage effects such as corona and arc-over. These large sizes often result in modification being an expensive and time-consuming process.

For the 60-kV facility, high-speed current and voltage monitors are in place and the capability of viewing the current distribution at the anode is available. The voltage and current monitors of the 500-kV system were not constructed because final electrode configurations are undetermined. The vacuum systems of both facilities are fully operational, including residual gas monitoring. The facilities are not presently in use because budgetary constraints forced termination of the effort.

REFERENCES

1. G. Bekefi, Ed., *Principles of Laser Plasmas* (John Wiley and Sons, New York, 1976).

2. P. J. Tallerico, "The Lasertron RF Generator for FEL Applications," Nucl. Instrum. Meth. Phys. Res. *A272*, 218 (1988).

3. R. L. Sheffield, E. R. Gray, and J. S. Fraser, "The Los Alamos Photoinjector Program," Nucl. Instrum. Meth. Phys. Res. *A272*, 222 (1988).

4. M. Yoshioka, "Lasertron: A Pulsed RF Source Using a Laser-Triggered Photocathode," Jap. J. Appl. Phys. *28*, 1079 (1989).

5. Kalrez, a perfluoroelastomer, is a registered trademark of E. I. DuPont de Nemours and Co., Wilmington, DE. For vacuum properties, see M. F. Zibielski and P. R. Blasjuk, "Vacuum Evaluation of a New Perfluoroelastomer," J. Vac. Sci. Technol. *13*, 644 (1976).

6. G. N. Glasoe and J. V. Lebacqz, Eds., *Pulse Generators* (McGraw-Hill, New York, 1948).

7. A. E. Stappaerts, "A Novel Analytical Design Method for Discharge Laser Electrode Profiles," Appl. Phys. Lett. *40*, 1018 (1982).

8. Macor is a machinable glass-ceramic manufactured by Corning Glass Works.

9. Manufacturer's Data 1984 Catalog (Harshaw/Filtrol Partnership, 6801 Cochran Road, Solon, OH 44139).

10. Suitable single-ended coils are available from T & M Research Products, Inc., 139 Rhode Island St. NE, Albuquerque, NM 87108.

11. Westinghouse ABB, T & D Components Division, CGIT Laboratory, 25 Bridle Lane, Westboro, MA 01581.

12. Viton, a fluoroelastomer, is a registered trademark of E. I. DuPont de Nemours and Co., Wilmington, DE.

13. Impulse Engineering, Inc., 27 Village Lane, Wallingford, CT 06492.

14. R. H. Fowler, "The Analysis of Photoelectric Sensitivity Curves for Clean Metals at Various Temperatures," Phys. Rev. *38*, 45 (1931).

15. L. A. DuBridge, "A Further Experimental Test of Fowler's Theory of Photoelectric Emission," Phys. Rev. *39*, 108 (1932).

16. A. H. Sommer, *Photoemissive Materials* (John Wiley and Sons, New York, 1968).

17. P. N. J. Dennis, *Photodetectors, An Introduction to Current Technology* (Plenum Press, New York, 1986).

18. H. B. DeVore and J. W. Dewdney, "Photoconductivity and Photoelectric Emission of Barium Oxide," Phys. Rev. *83*, 805 (1951).

☆ U.S. Government Printing Office: 1992—648-127/62429